Role of spinal sensorimotor circuits in triphasic command: a simulation approach using Goal Exploration Process.

Daniel Cattaert[1], Matthieu Guemann[1], Florent Paclet[1], Bryce Chung[2], Pierre-Yves Oudeyer[3], Aymar de Rugy[1]

[1] Institut de Neurosciences Cognitives et Intégratives d'Aquitaine,

UMR 5287 CNRS & Univ. Bordeaux, Bordeaux, France

[2] Neuroscience Institute, Georgia State University, Atlanta, GA 30302

[3] Inria Bordeaux Sud-Ouest, Talence, France ;

Corresponding author: Daniel Cattaert

INCIA UMR 5287 – 146 rue Léo Saignat, 33076 BORDEAUX CEDEX, France

Manuscript type: Research article

Word count: 12 379

Abstract

During rapid voluntary limb movement about a single joint, a stereotyped triphasic pattern is typically observed in the electromyograms (EMGs) of antagonistic muscles acting at this joint. To explain the origin of such triphasic commands, two types of theories have been proposed. Peripheral theories consider that triphasic commands result from sensorimotor spinal networks, either through a combination of reflexes or through a spinal central pattern generator. Central theories consider that the triphasic command is elaborated in the brain. Although both theories were partially supported by physiological data, there is still no consensus about how exactly triphasic commands are elaborated. Moreover, capacities of simple spinal sensorimotor circuits to elaborate triphasic commands on their own have not been tested yet. In order to test this, we modelled arm musculoskeletal system, muscle activation dynamics, proprioceptive spindle and Golgi afferent activities and spinal sensorimotor circuits. Descending step commands were designed to modify the activity of spinal neurons and the strength of their synapses, either to prepare (SET) the network before movement onset, or to launch the movement (GO). Since these step commands do not contain any dynamics, changes in muscle activities responsible for arm movement rest entirely upon interactions between the spinal network and the musculo-skeletal system. Critically, we selected descending step commands using a Goal Exploration Process inspired from baby babbling during development. In this task, the Goal Exploration Process proved to be very efficient. It proficiently discovered step commands that enabled spinal circuits to handle a broad spectrum of functional behaviors. Notably, this accomplishment was predominantly realized while eliciting natural triphasic commands, thereby substantiating the inherent capacity of the spinal network.

Author Summary

In this study, we tested the capacities of sensorimotor spinal networks and musculo-skeletal dynamics to produce triphasic commands for single joint arm flexion. Spinal networks only received step commands from the brain consisting in preparatory (SET) and launch (GO) controls. In the absence of dynamics in these descending commands, the arm movements result solely from sensorimotor interactions and processing in the spinal circuits. Descending commands were elaborated in a Goal Exploration Process (GEP) inspired from baby babbling during development. We show that in this configuration, sensorimotor spinal networks spontaneously produce triphasic commands for most arm flexion movements in a large range of amplitudes and speeds.

Introduction

During rapid voluntary limb movement about a single joint, a stereotyped triphasic pattern is observed in the electromyograms (EMGs) of antagonistic muscles commanding this joint (Hallett et al. 1975). Prior to limb displacement, the agonist muscle is briefly active (AG1). After the limb begins to move, a burst of muscle activity occurs in the antagonist muscle (ANT) while the agonist is silenced, and then a second burst is observed in the agonist (AG2). The precise organization of this triphasic pattern ensures the softness of the movement.

What is the origin of this triphasic command? Two possibilities have been proposed; either a **spinal origin** via sensorimotor circuits (Barnett and Harding 1955; Ghez and Martin 1982; Terzuolo et al. 1974) or a **central origin** elaborated in brain networks and transmitted to the spinal cord via descending commands. The **central hypothesis** was supported by observations on humans with severe, though not complete, sensory neuropathy, who could still produce triphasic patterns **(Hallett et al. 1975; Rothwell et al. 1982**). Although these studies highlight the capacities of the motor cortex and other higher centers that can learn how to control limb movements after partial or total deafferentation, the deep reorganization of motor commands following such deafferentation prevents firm conclusion about how triphasic commands are produced in healthy subjects. Other studies used reversible transient deafferentation using ischemic process of the muscles controlling the joint and their afferent nerves Ia and Ib, the diameter of which are more sensitive to ischemia that axons of alpha motoneurons (**Sanes and Jennings 1984**). During such reversible ischemia, the triphasic pattern persists, although passive movements fail to elicit stretch reflexes.

Other experiments indicate that triphasic motor command is also present in the primary motor cortex (M1), and that neural activities in M1 are correlated with output kinematics and kinetics during isometric-force and arm-reaching tasks (**Sergio et al. 2005**).

Physiological model describing the transformation from the neural activity in M1, through the muscle control signal, into joint torques and down to endpoint forces and movements (**Trainin et al. 2007**), show that optimized solutions for M1 activities display triphasic changes in temporal pattern and instantaneous directionality similar to that found in the EMG (**Trainin et al. 2007**). Other studies have also suggested that optimal control models can predict EMG patterns in step-tracking wrist movement (**Haruno and Wolpert 2005**), and even triphasic pattern of muscle activation (**Ueyama 2021**). Interestingly, such optimal control models also predict neural representation in M1 (**Ueyama 2021**).

In opposition with the arguments in favor of a central origin of triphasic commands, it was shown that procedures that modify discharge of muscle spindle afferents during movement alter the duration and amplitude of these bursts **(Brown and Cooke 1981; Hallett and Marsden 1979**). In addition, simulation studies concerning the central origin of triphasic commands, although aiming toward physiological models, often lack spinal sensorimotor loops (**Trainin et al. 2007**). Therefore, if we cannot doubt that M1 neurons and populations of neurons present activities correlated with kinetic, kinematic and dynamic cues of the performed movements, there is still questions about the possible role of spinal sensorimotor circuits in the elaboration of triphasic commands. More precisely, if the first EMG activity (AG1) can be attributed to a central command from the brain (at least for its onset), there is still debate about ANT and AG2.

The first aim of this paper was to explore the capacities of the spinal sensorimotor circuits in shaping triphasic commands, using a modeling approach based on the neuromechanical environment AnimatLab (https://www.animatlab.com/). We modelled the movement of the forearm around the elbow joint, involving two muscles (biceps and triceps). Movements consisted in elbow flexion starting from a fully extended position. Our approach was based on spinal like regulator (SLR) work (**Raphael et al. 2010**). Spinal interneurons and synapses of sensorimotor circuits were controlled by simple descending

SET and GO step commands. The SET commands shape the sensorimotor circuits (synaptic gains, level of activity of neurons) without producing any movement, and the GO commands trigger and elicit the movement. These signals, deprived from any dynamic content, were chosen in order to give the spinal sensorimotor circuit the complete responsibility in the shaping of the dynamics of the commands, and in particular the production of the triphasic commands.

We also wanted the neuromechanical system to self-organize its commands as a function of the produced movements, as would do a child exploring the commands of its own arm. Recent advances in developmental machine learning **(Baranes and Oudeyer 2013; Forestier et al. 2017**) have shown that a novel form of exploration algorithms, called *Goal Exploration Processes* (**GEP**), can be used to automatically define target behaviors and efficiently discover a map of reachable behaviors, thereby solving problems of unreachable behaviors and local minima encountered by alternative, state-of-the-art optimization methods **(Colas et al. 2018; Forestier et al. 2017; Oudeyer and Kaplan 2007) ;** (for related methods using diversity search to solve problems with local minima or sparse rewards, see also **Eysenbach et al. 2019; Lehman and Stanley 2011; Mouret and Doncieux 2012; Pathak et al. 2017)**. Moreover, self-conducted exploration of high-dimensional, continuous parameter systems have the advantage to be sample efficient, i.e., they enable the discovery of diverse behavioral domains with a limited number of experiments. So far, such algorithms have been used to discover diverse behaviors in robotics **(Forestier et al. 2017; Péré et al. 2018)** as well as in complex systems such as cellular automata, morphogenetic models **(Etcheverry et al. 2020; Reinke et al. 2019**) and chemical systems (**Grizou et al. 2020**), implementing a form of discovery assistant that can leverage interactively guidance of users (**Etcheverry et al. 2020**).

The second aim of the present work was to extend the application domain of such algorithms by studying their efficacy when applied to neuromechanical systems. We used a

132 simple GEP protocol inspired from **Forestier et al (2017)**. These algorithms use two work
133 spaces: (i) one for the behaviors: here we used a two dimensions space (movement
134 amplitude and movement speed), and (ii) one for the parameters that determine the motor
135 commands from the brain: here we used a series of step commands that modify synaptic
136 strength and neuron activity in spinal cord circuits either in the preparatory phase (SET) or to
137 launch the movement). The GEP finds new valid behaviors by repeating 4 stages:

138 1- Choose a goal (a goal is a targeted behavior)
139 2- Find the parameters that produced a behavior close to the aim in the data base of
140 preceding successes and modify slightly these parameters in a random way
141 3- Run the model with these parameters
142 4- Observe the result and if acceptable, store behavior and parameters in the
143 database.

144 Several modelling approaches have proposed that the CNS employs a minimum jerk
145 strategy when planning any given movement (**Flash and Hogan 1985**). This proposal was
146 refined later **(Nakano et al. 1999)** showing that minimum angle jerk predicts the actual arm
147 trajectory curvature better than the minimum jerk model. Therefore, we used it here. Once
148 valid behaviors were found, the GEP searched new ones by modifying preexisting valid
149 behaviors. Valid behaviors, the parameter sets of which were altered to elaborate new
150 commands, were chosen on the periphery of the behavior domain in order to extend it.
151 Because the policy was random, we called this process rGEP. Here, the rGEP proved efficient
152 at discovering step commands that enabled spinal circuits to handle a broad spectrum of
153 functional behaviors while predominantly eliciting natural triphasic commands.

154

155 # Results

156 ## A. Goal exploration process explores the capacity of spinal sensorimotor
157 circuits and their descending commands to produce behaviors.

158 In this section, we provide a brief overview of the neuromechanical models and the
159 process (rGEP) used to explore their behavioral capabilities.

160 ### *1. Example of a simple Neuromechanical model*

161 Neuromechanical model of musculoskeletal apparatus and spinal sensorimotor
162 networks were modelled on the AnimatLab platform (see Methods). All neurons modelled in
163 this study were non-spiking (NS) neurons (i.e., neurons that do not produce spikes but
164 transmit activity to postsynaptic neurons in a continuous manner when their potential is
165 over a threshold value - see Methods for more explanations). Such neurons present the
166 advantage to avoid discontinuity of spikes and spiking synaptic transmission. This is specially
167 critic in small neuron networks, when the level of activity is low.

168 To illustrate how rGEP works and progresses along time, we have chosen the simplest
169 network, which contained only 6 neurons and 6 synapses, and is controlled by 14 descending
170 commands (Figure 1B). Using this model, we will see how rGEP progressively builds a
171 behavior map (i.e., the collection of all valid behavior found) and parameter maps (i.e., the
172 collection of their associated 14 parameters' sets).

173 In this study, one of the objectives was to demonstrate how a highly simplified
174 sensorimotor system (Figure 1B) could proficiently manage movement control, as previously
175 shown by **Raphael et al. (2010)** in the context of more complex spinal networks. The specific
176 aim here was to generate minimum jerk movements. Therefore, we used the same
177 principles for descending commands as **Raphael et al. (2010)**. Descending commands were
178 represented as step functions starting at t=1s (SET command) and at t=5s (GO command)
179 (Figure 1C). The SET commands were responsible for the state of readiness of the network.

This first stimulation should activate the network without releasing any movement **(Eliasmith and Anderson 2003**); (**Prut & Fetz, 1999**).

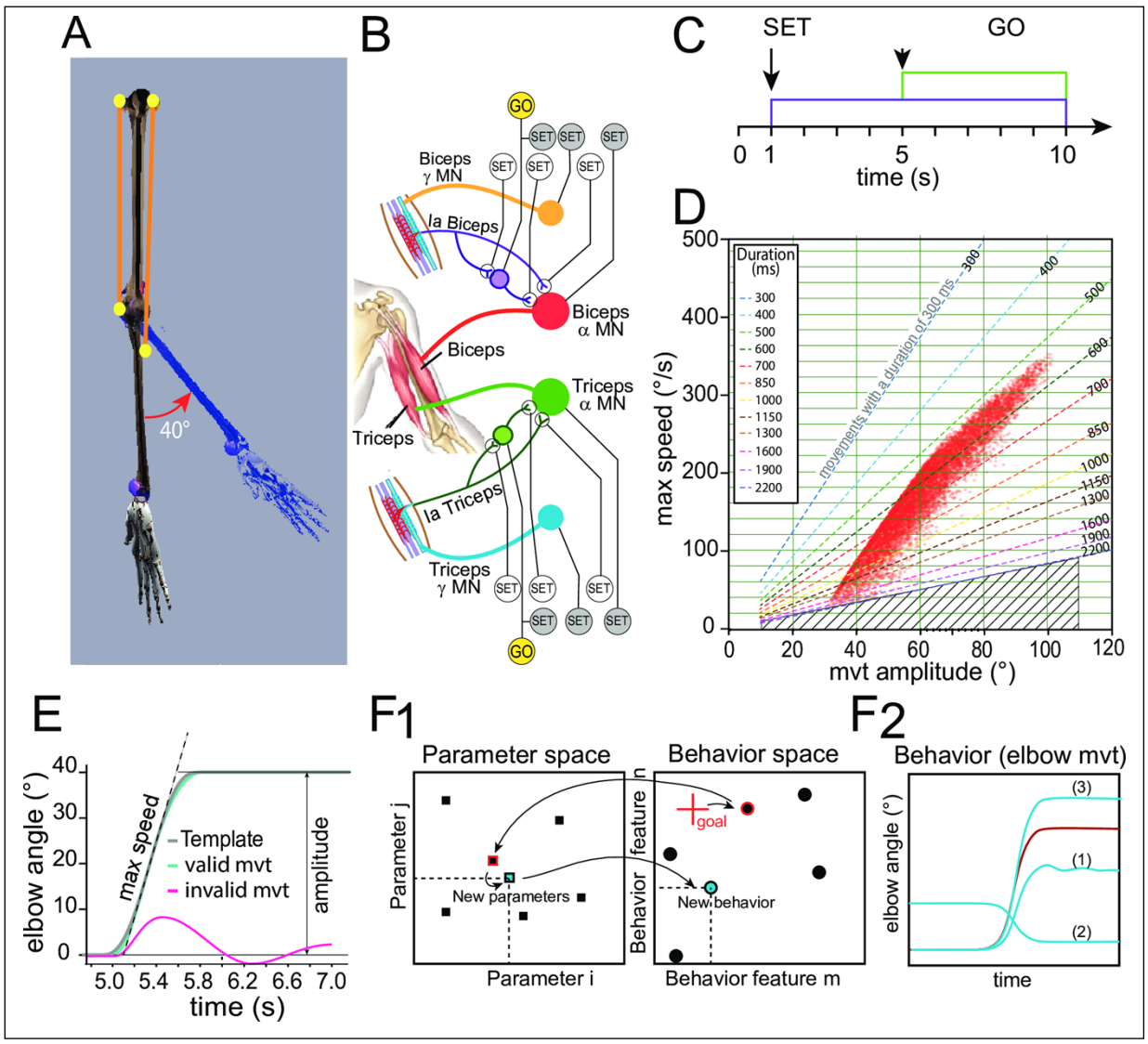

Figure 1: Simplified neuromechanical model and GEP principles.

A, Musculoskeletal system.

B, Simplified sensorimotor system comprising αMNs, γMNs, propriospinal interneurons and Ia afferents from muscle spindles, with SET ad GO commands. In this study, more complex sensorimotor networks have been associated to the same musculo-skeletal system (see Figs 3-9).

C, SET and GO commands used to control the sensorimotor network. The SET commands adjust all neuron activity levels at 1 sec to bring the network in a state ready to trigger the movement (without producing the movement by itself). The GO commands launch the movement. SET and GO commands are the parameters of **parameter space**.

D, Example of Behavior space obtained with rGEP algorithm after 91794 iterations. Valid behaviors are indicated by red dots, and corresponding movement durations are indicated by doted lines.

E, In this work the **behavior space** was defined by the amplitude of elbow movement (abscissa) and its maximal speed (ordinate).

F, Schematic diagram of the GEP exploration algorithm. **F1**: Process starts from an existing **parameter space** (black filled squares in *Parameter space* – for simplicity reduced to two parameters), which is associated with a **behavior space** (black filled circles in *Behavior space*), a new *goal* is given in the periphery of the known behavioral space (red cross). The algorithm searches for the closest behavior (closest neighbor), it will retrieve the parameters associated with this behavior and replay its parameters including additional noise (*"New parameters"*). This new set of parameters generates a *"New behavior"* in the space of behaviors that is kept or not, depending on its *Cost* value). **F2**: The movement that was closest to the goal (red circle in behavior space, and red movement trace in right diagram) is a valid movement. However, when its parameters are changed

randomly different issues are possible: i) the obtained new movement is invalid, either because there are oscillations (1) or because it is performed in the wrong direction (2); ii) the new movement is valid and may be close or far from its parent.

The SET command targeted all the elements of the network (neurons and synapses) and their control was maintained constant during all the time of the simulation (up to t=10s). The GO commands were responsible for movement initiation and were maintained constant until the end of the simulation. In this example GO commands modulated the level of activity of propriospinal interneurons (see Figure 1B). Note that at t = 5 seconds, the transient changes induced by the SET command had stabilized before the GO command was issued.

2. Brief overview of rGEP

To assess behavior capabilities associated with a given neuromechanical model (i.e., the variety of movements that can be produced (Figure 1D) and meeting some criteria like minimum jerk - see methods for the cost function), we have developed a rGEP algorithm that uses two spaces (the parameter space and the related behavior space). The movements contained in the behavior space are defined by their amplitude and their maximal speed (Figure 1E). At each iteration, goals (i.e., movements of given amplitude and speed) are self-produced by the algorithm. Goals are disposed either on the periphery of (extend strategy) or inside (fill strategy) the known behavior space. In the illustration of Figure 1F1, the example goal is on the periphery of the behavior domain (see red cross). The closest behavior is then searched and its associated parameters are slightly modified (**random function**) to produce a new parameter set (*New parameters*). We choose a random policy in order not to introduce bias in the setting of new values for parameters. Because the policy used by GEP for parameter changes was a random function, this GEP was named **rGEP.** After a simulation is run (Figure 1F2), if the produced movement fulfils the **acceptance criteria**, it is stored in the behavior domain (see trace (3) in Figure 1F2), otherwise, it is rejected (traces

230 (1) and (2)). Acceptance criteria were as follows: (i) the produced movement should fit a
231 **minimum jerk angular kinetics** (**Friedman and Flash, 2009**); (ii) there should be no
232 oscillations in preparatory and post movement phases; (iii) the movement amplitude should
233 be in the range (10-110°); (iv) no co-contraction should be present in the preparatory phase
234 (controlled by SET commands, see below). A **cost function** ensured valid behaviors fulfill
235 acceptance criteria (see methods)

236 Because rGEP needs valid behaviors to progress, the first step, was to find initial valid
237 behaviors. In order not to interfere with the design of the commands, these initial behaviors
238 (termed **seeds**) were found via optimization methods (covariance matrix association
239 evolution strategy (CMAes) or variable step coordinate descent (VSCD) – see methods).
240 Briefly, a desired behavior (a movement template) was given to the optimization method
241 that worked on the parameters of the SET and GO commands to find the result that best
242 fitted the desired movement template. During this process of optimization, any valid
243 movement produced was stored and could be used as a seed.

244 *3. Time course of the rGEP algorithm*

245 An example of rGEP time course is presented in Figure 2, on the same simple model
246 presented in Figure 1 (see also inset network diagram in Figure 2). Before rGEP starts, **valid**
247 **behaviors (seeds)** must be given to the algorithm (see below). In the example presented in
248 figure 2, six seeds were given (see blue crosses in Figure 2A1-4).

249 Four pictures of the behavior domain extension are presented for 100, 500, 1000 and
250 4000 valid behaviors (Figure 2A1-4), corresponding to 239, 1232, 2440 and 9922 runs of
251 simulation, respectively. As the rGEP progresses, the behavior domain extends (Figure 2B,
252 violet trace, *behavior domain area*). The behavior domain area was quantified as the number
253 of cases of a grid, defined in the behavior work space (see Methods), which contain at least
254 one valid behavior (see green grids in Figure 2A1-4).

While the borders of the behavior domain get more and more precise, there were still some empty central zones when the process was stopped after 1000 “extend” rounds and 50 “fill” rounds (totalizing #150000 runs). Note that there is no direct relationship between the number of extend rounds and the number of runs, because the number of runs in a given round depends on the size of the behavioral domain at the time the round is launched. Note also that the empty zones were still being progressively explored when rGEP was stopped. Indeed, , the process was not complete in this example as the behavior domain area was still increasing, and did not reach a steady state (Figure2B).

We can also see that the progression of rGEP is not linear. Indeed, several transient plateaus were observed (see filled arrow heads in Figure 2B) on the behavior domain area curve (violet trace). During such blockage of exploration, valid results were found in the already discovered behavior domain, resulting in a transient increase of the mean density (see methods) of valid behaviors (green curve in Figure 2B). The situation unblocks when an original valid behavior is found that extends the behavior domain, and allows new behaviors to be found from its parameter set, resulting sometimes in an abrupt increase of the behavior domain area (see open arrow heads in Figure 2B) while the mean density decreases (see green trace, in Figure 2B). As the behavior domain extends (Figure 2A-B), the parameter domain also evolves, and the final parameter domain is presented in Figure 2C1-7. In this figure, all valid values of the 14 parameters are presented in 7 graphs, each displaying a pair of parameters: GO stim: [*Triceps PN, Biceps PN*] (Figure 2C1); SET stim: [*Triceps PN, Biceps PN*] (Figure 2C2), [*Triceps Alpha, Triceps Alpha*] (Figure 2C3), [*Triceps Gamma, Biceps Gamma*] (Figure 2C4); SET syn: [*Triceps 1a-> Alpha*, *Biceps 1a->Alpha*] (Figure 2C5), [*Triceps PN->Alpha, Biceps PN->Alpha*] (Figure 2C6), [*Triceps 1a- >PN, Biceps 1a- >PN*] (Figure 2C7) in which *stim* = stimulus sent to a neuron, and *syn* = strength setting of a synapse between a presynaptic and a post synaptic neuron separated by “->” (see Figure2 legend for more explanations).

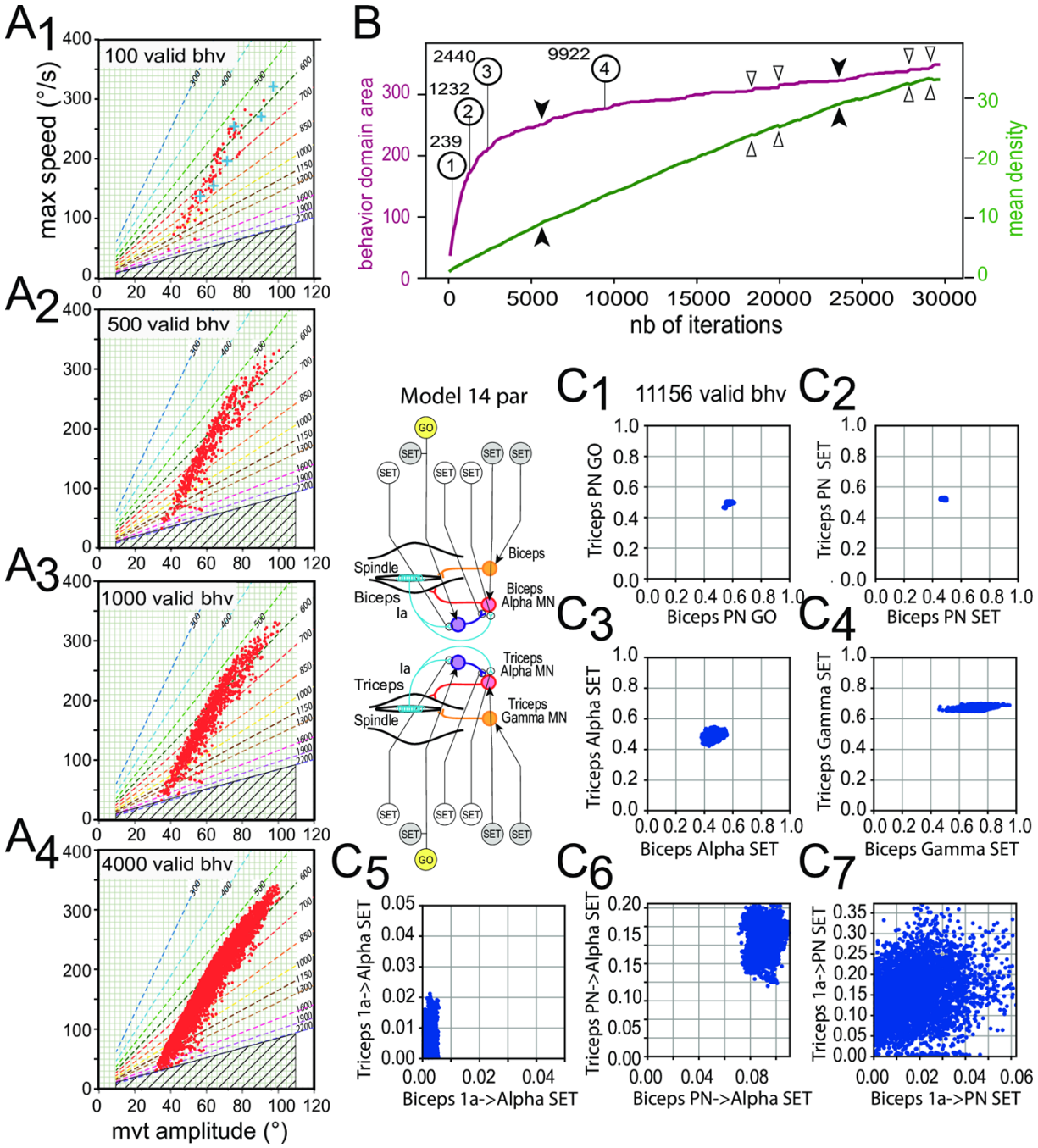

Figure 2: Temporal evolution of rGEP. **A**, Progression of the behavior domain uncovered by rGEP after 100 (A1), 500 (A2), 1000 (A3) and 4000 (A4) valid behavior were found. **B**, Time course of behavior domain area expansion (i.e., number of squares containing at least one valid behavior in the green grids presented in A1-4) presented in violet trace. The mean density of behaviors in the behavior domain area is presented in green trace. The numbers 1, 2, 3 and 4 correspond to the behavior domains representations shown in (A). **C**, Parameter domain. The 14 parameters are represented in 7 graphs displaying 2 parameters each: 4 stimulus graphs (C1-4) and 3 synapse strength graphs (C5-7) obtained after 91794 runs. Axis names: stimulus graphs represent intensity of stimulus sent to a neuron in the GO (C1) and SET (C2,3,4) commands; synapse strength graphs represent strength setting of a synapse between a presynaptic and a post synaptic neuron separated by "->". Since in this example the Triceps and the Biceps networks are separated, for simplification the name of the network is given first followed by pre- and post-synaptic elements (for example Biceps 1a->Alpha SET indicate the SET command for synaptic strength between 1a spindle afferent and alpha MN both belonging to the Biceps network). The six seeds used to launch the rGEP are indicated with blue cross in the behavior map A1. **Inset**: Diagram of the neuron network model used in this rGEP.

281

282 *4. Behavior domain of the complete (50-parameters) model with both Ia and Ib*
283 *afferents and associated networks*

284 We started the exploration with a system receiving proprioceptive feedback from
285 muscle spindles (Ia) and Golgi Tendon Organ (GTO). The associated sensorimotor circuits
286 were inspired from Raphael et al (2010), and contained 12 neurons (2 alpha motoneurons
287 (MNs), 2 gamma MNs, 2 propriospinal interneurons (INs), 2 Ia INs, 2 Ib INs, and 2 Renshaw
288 INs), and 30 synapses. GO commands targeted the 8 INs, SET commands targeted the 12
289 neurons and adjusted the 30 synapses' gains (Figure 3A).

290 The behavior domain found for this 50 parameters model by the rGEP is presented in
291 Figure 3B after 1500 rounds of "extend" and 100 rounds of "fills" totalizing 107315 runs, in
292 which 36152 behaviors were valid. The behavior domain is defined by two parameters of the
293 produced movements: maximal speed (ordinate) and movement amplitude (abscissa). A
294 third characteristic of movements (movement duration) is presented on the graphs by
295 oblique lines labelled with the represented duration (in ms). Only physiologically plausible
296 movements have been retained (slow movements the duration of which was > 2s have been
297 rejected – see gray area). Only movements with an amplitude in the range [10°, 110°] have
298 been retained, to avoid too small movements and too large movements that could reach the
299 flexion limits. With both Ia and Ib sensorimotor circuits complete, this model could perform
300 large movement (>80°) at a rapid speed (>400°/s) with movement durations < 400ms. Note
301 for each amplitude, a great variety of speeds was found.

302 A representative example of a large movement (amplitude 90.23°) is given in Figure
303 3C1. Note the profile of the movement that fitted a minimum jerk profile with small MSE
304 value (0.59). Several other variables are also presented for this example: Force, Membrane
305 potentials of MNs, and sensory neurons. At the initiation of the movement, the force
306 recorded in the Biceps was large (reaching 150 N) and decayed slowly during 200 ms, and

more rapidly during the next 200 ms (Figure 3C2). The force recorded in the triceps increased during the rapid decrease of biceps force, and reached 102 N at t=540ms, and then decreased in the last part of flexion movement. After movement stopped, triceps force slowly increased again, while biceps force slightly increased, resulting in a stable global torque that maintained the forearm in a stable position.

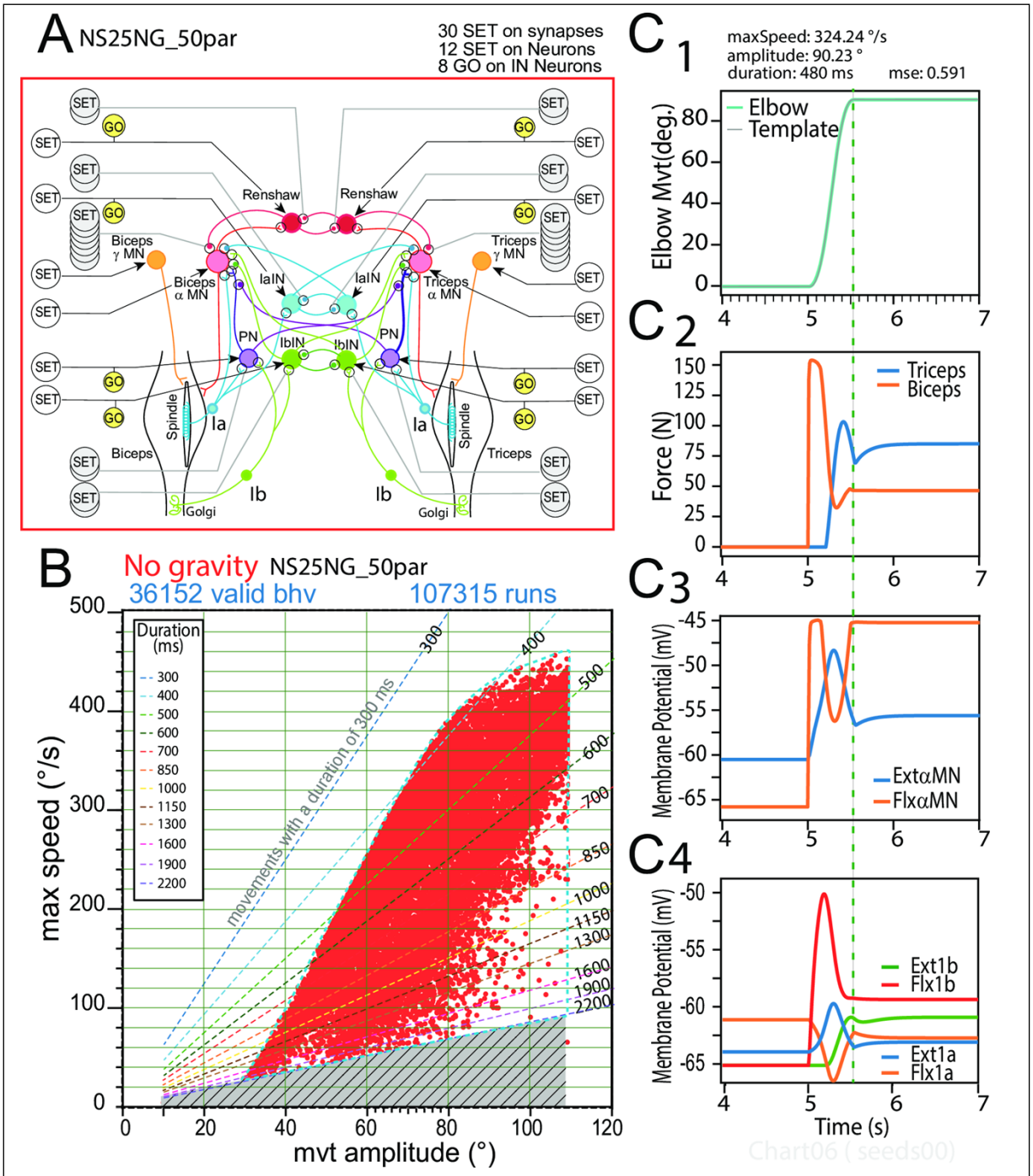

Figure 3: Movements produced by rGEP with the 50-parameters model. **A**, Sensorimotor spinal network of the 50-parameters model. **B**, Behavior domain uncovered by rGEP on this model. The perimeter of the domain is outlined with a blue dashed line. **C**, Representative example of one valid movement in the behavior domain.

312 The activity of alpha MNs present transient activities during the movement phase:
313 the biceps MN (*FlxαMN*) presents two peaks of depolarization, the second being hardly
314 visible, and an abrupt decrease of activity between the two peaks, during which the triceps
315 MN (*ExtαMN*) presents a peak of activity (Figure 3C3). Once the flexed position is reached,
316 the activity of both alpha MNs remain stable. During the movement phase, the
317 proprioceptive feedback from Ib afferents was much larger than that of the Ia afferents
318 (Figure 3C4). The shape of Ib activations was also different from that of Ia afferents: during
319 the rapid flexion movement, the Ib activity of the flexor muscle (*Flx1b*) present a large peak
320 during the acceleration of the flexion movement, in accordance with its role in sustaining the
321 flexion movement via the Flexor PN excitatory circuit (see Figure 3A); this initial *Flx1b* peak is
322 followed by a smaller peak of the extensor 1a activity (*Ext1a*) that contributes to slow down
323 the flexion movement due to its excitatory effect on the extensor αMN (see Figure 3A); this
324 slowing effect is prolonged by the delayed increase of *Ext1b* activity that activates the
325 extensor αMN via the PN interneuron of the extensor circuit (see Figure 3A), with a small
326 peak just before movement's end; Ext1b activity is maintained after the end of the flexion
327 movement. Note that during the flexion movement, the activity of the Flx1a presents a
328 trough.

329 The time course of 1a and 1b afferent activities (larger Flx1b peak followed by a
330 smaller Ext1a peak, and by a delayed step-like increase of the Ext1b activity, concomitant
331 with the recovery of Flx1a trough) were regularly observed in the 50-parameter model, with
332 some small variations all along its behavior domain. However, in the same domain regions,
333 other profiles coexisted, with more irregularities similar to that observed in the absence of
334 1a afferent feedback (see below, §7). This first study will serve to compare the capacities of
335 other models issued from this one, but lacking some neural elements. To facilitate
336 comparison, the perimeter of the behavior domain of the 50-parameter model (see dashed
337 blue line in Figure 3B) will be superimposed on their behavior domains.

338 *5. Behavioral domain produced in the absence of Ib feedback (with central cross*

339 *connections).*

340 In order to study what proprioceptive feedback was necessary to produce valid

341 movements, in a first step, we suppressed the Ib input, the Ib INs and their synapses (Figure

342 4A). When rGEP was run on this model, the resulting behavior domain was close to the one

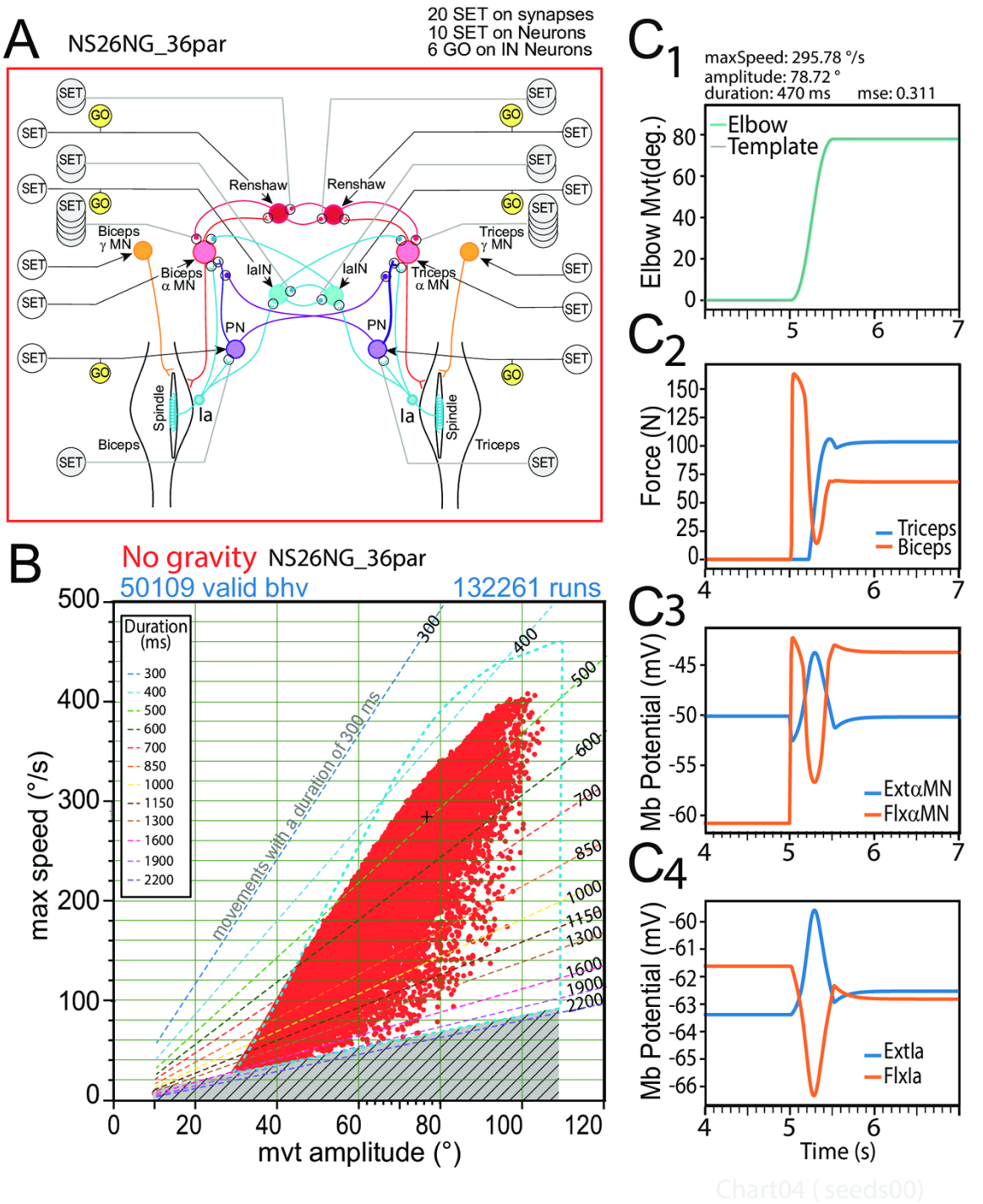

Figure 4: Movements produced by rGEP with the 36 parameters model. **A**, Sensorimotor spinal network of the 36 parameters model. **B**, Behavior domain uncovered by rGEP on this model. For comparison, the perimeter of the domain of the 50-parameter domain is represented with blue dashed line. **C**, Representative example of one valid movement in the behavior domain.

343 obtained with the complete spinal network (compare Figure 3B and Figure 4B), although
344 maximal speed for large movements was slightly reduced, and all movement durations were
345 longer than 420 ms.

346 Forces, MN activities and muscle spindles feedback (Figure 4C) were very similar to
347 that of the complete model (Figure 3C) for comparable movements. A representative
348 example of a large movement (amplitude 78.72°) is given in Figure 4C1, with a maximal
349 speed of 295.78°/s, the amount of force developed by the Biceps muscle (Figure 4C2) was in
350 the same range (#150 N) as that observed for the complete model. This is also true for MN
351 and 1a activities (Figure 4C3-4).

352 *6. Behavioral domain produced in the absence of Ib feedback (without central cross*
353 *connections).*

354 To go further in the analysis of the involvement of Ia proprioceptive feedback in the
355 production of minimum jerk movements, we drastically reduced the sensorimotor network,
356 by suppressing all relationships between extensor and flexor parts of the network, as well as
357 all interneurons except propriospinal INs. The resulting spinal network was the 14-
358 parameters simplified network presented in Figure 1B, and redrawn in Figure 5A with the
359 same design as other models presented in Result section. Interestingly, this extremely
360 simplified spinal network, reduced to Ia proprioceptive inputs connecting their homonymous
361 MN either directly or via their propriospinal IN (PN), was capable of producing a great variety
362 of valid behaviors (Figure 5B). The resulting behavior domain was, however much smaller
363 than the one of the 36-parameters mode (no movement shorter than 500 ms were produced
364 and maximal speed was under 370°/s). A representative example of a large movement
365 (amplitude 80.58°) is given in Figure 5C1.

366

367

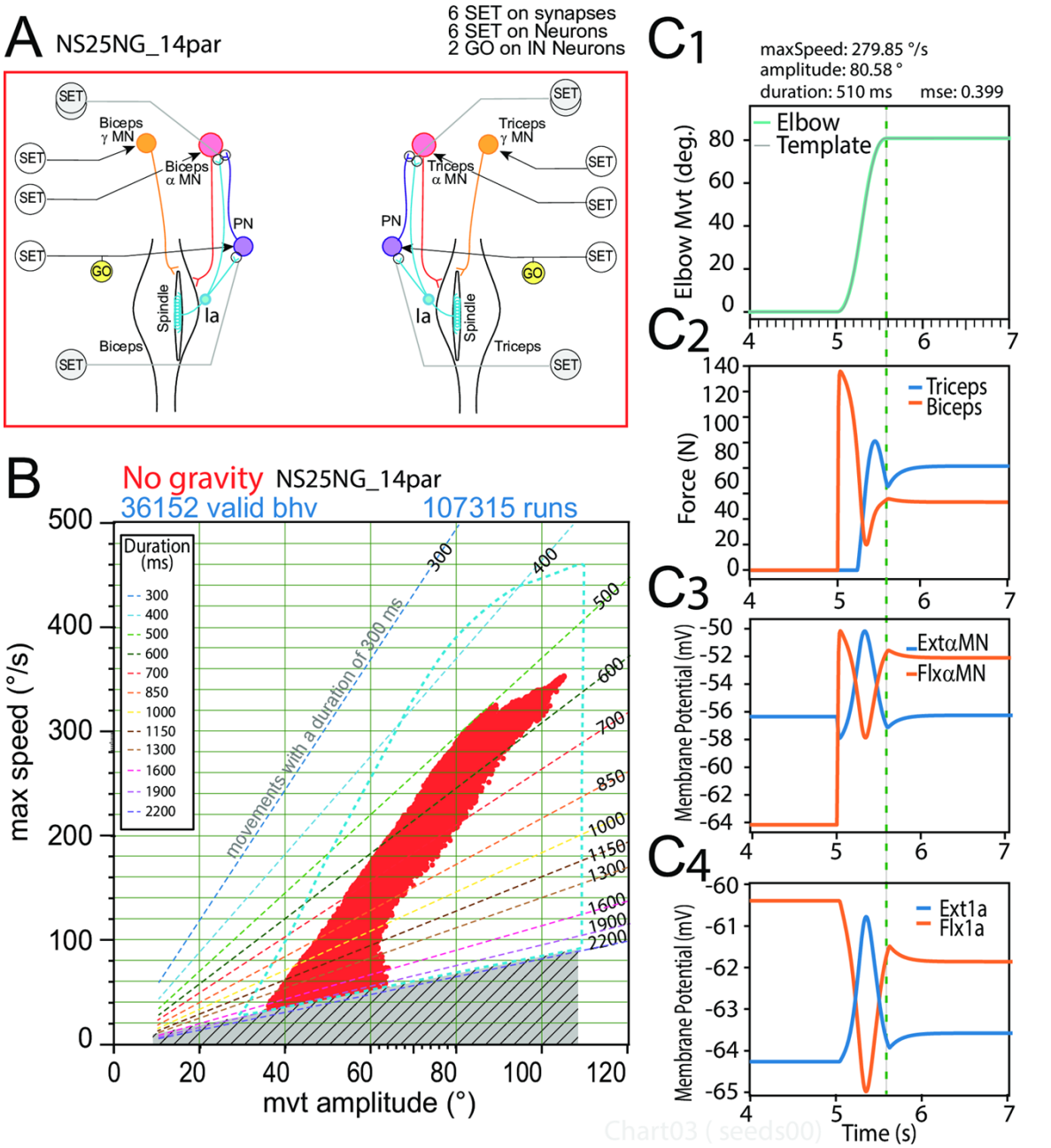

Figure 5: Movements produced by rGEP with the 14-parameters model. **A**, Sensorimotor spinal network of the 14 parameters model. **B**, Behavior domain uncovered by rGEP on this model. For comparison, the perimeter of the domain of the 50-parameter domain is represented with blue dashed line. **C**, Representative example of one valid movement in the behavior domain.

7. Behavioral domain produced in the absence of Ia feedback with central cross-connections.

We then applied the same method to test Ib afferents involvement in the production of valid movements via rGEP. Starting from the complete (50-parameters model), we suppressed Ia afferents, Ia INs and their synapses (Figure 6A). This Ib network could produce

374 a variety of valid behaviors (Figure 6B), with fast movements of great amplitude (maximal
375 speed > 400°/s and movement duration < 450 ms. However, the behavioral domain was
376 significantly smaller than that of the 50-parameter model: for each amplitude, the maximal
377 speed observed in valid behaviors were always smaller than that of the 50-parameters
378 model (Figure 6B).

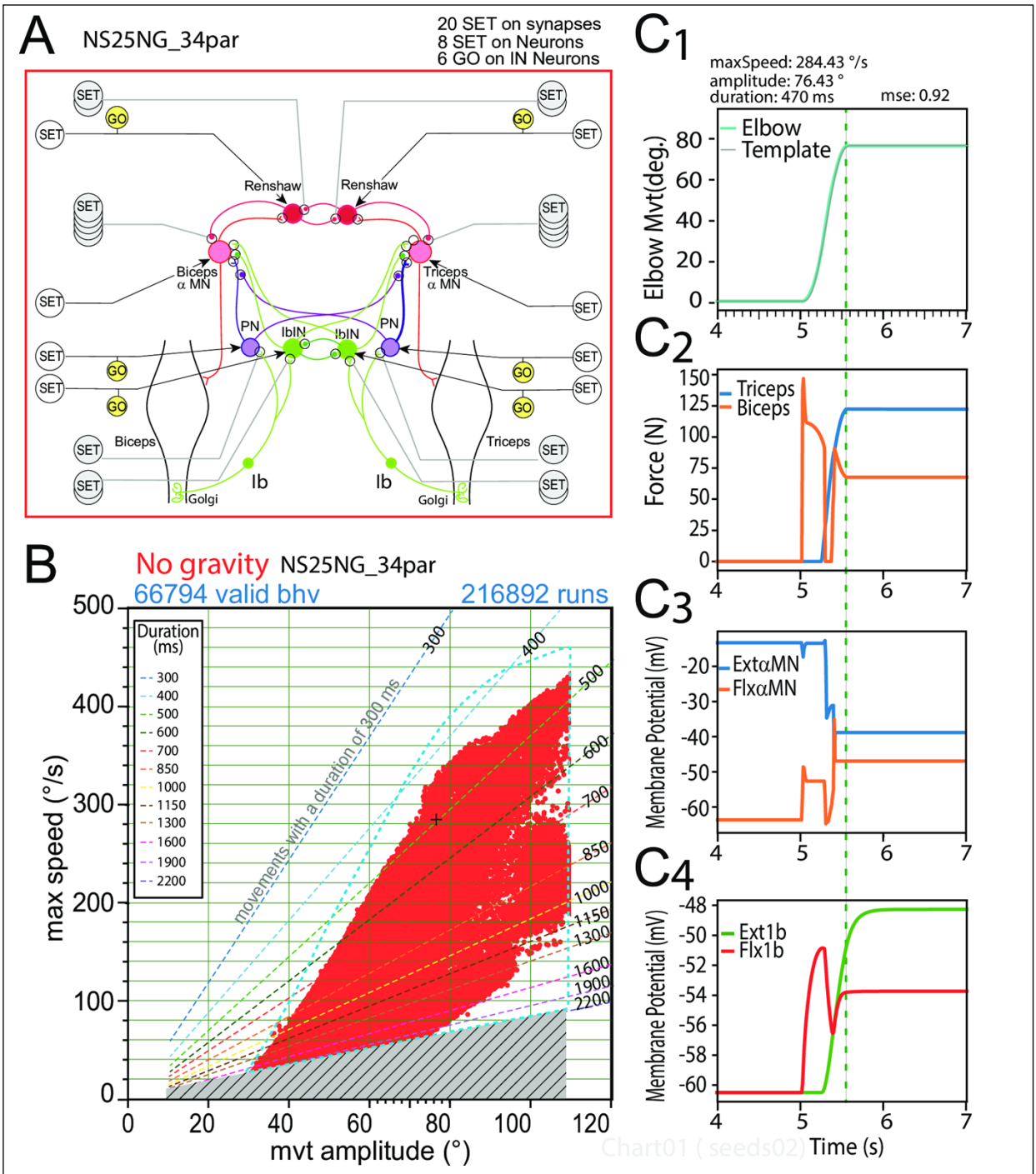

Figure 6: Movements produced by rGEP with the 34-parameters model. **A**, Sensorimotor spinal network of the 34 parameters model. **B**, Behavior domain uncovered by rGEP on this model. For comparison, the perimeter of the domain of the 50-parameter domain is represented with blue dashed line. **C**, Representative example of one valid movement in the behavior domain.

379 The limitations of the 34-parameters model were likely linked with the difficulty to get
380 stable control of neurons and forces when the only proprioceptive feedback comes from
381 Golgi Tendon Organs, as can be observed in Figure 6C. Note, in particular, the complex shape
382 of the force time course (Figure 6C2), with rapid increase at t=5s and rapid decrease at
383 t=5.3s, and in between an evolution that presents several changes. In other recordings,
384 these rapid changes correspond to oscillations that are also visible in the αMNs activity, and
385 in the Flexor Ib afferent activity although to a lesser degree (not shown). A characteristic of
386 this network is also visible in the activity of the αMNs (Figure 6C3) with the presence of
387 constant activity between t=5s and t=5.3s. We never found this type of activity in the models
388 with muscle spindles.

389 *8. Behavioral domain produced in the absence of Ia feedback with central cross-*
390 *connections limited to IbINs.*

391 We went further in the suppression of Ib sensorimotor elements (no Renshaw, no
392 cross connections from propriospinal INs), and we tested a spinal network in which Ib INs
393 were kept with their reciprocal connections (Figure 7A). The behavior domain found by rGEP
394 with this reduced Ib network was smaller than that of the 34-parameters. For each
395 movement amplitude, the maximum speed was more reduced than that of the 34-
396 parameters model, with a straight-line upper border (Figure 7B). It seems also that slow
397 movements were difficult to produce: there is no slow movements with amplitude larger
398 than 40 degrees in Figure 7B. An example of large movement (amplitude 81.08°) is given in
399 Figure 7C. Again, as was the case when 1a afferent were absent, the activity profiles of MNs
400 were complex, with peaks and plateaus. The initial Biceps force peak is very short and
401 followed by a plateau (Figure 7C2). Note that the same profile is also found in the flexor
402 alpha MN (*FlxαMN*) (Figure 7C3). The plateau-like αMN activity was also observed in Figure

6C3. Note also that large forces were observed: the Biceps displayed an initial 120 N short peak; and the Triceps reached 90 N.

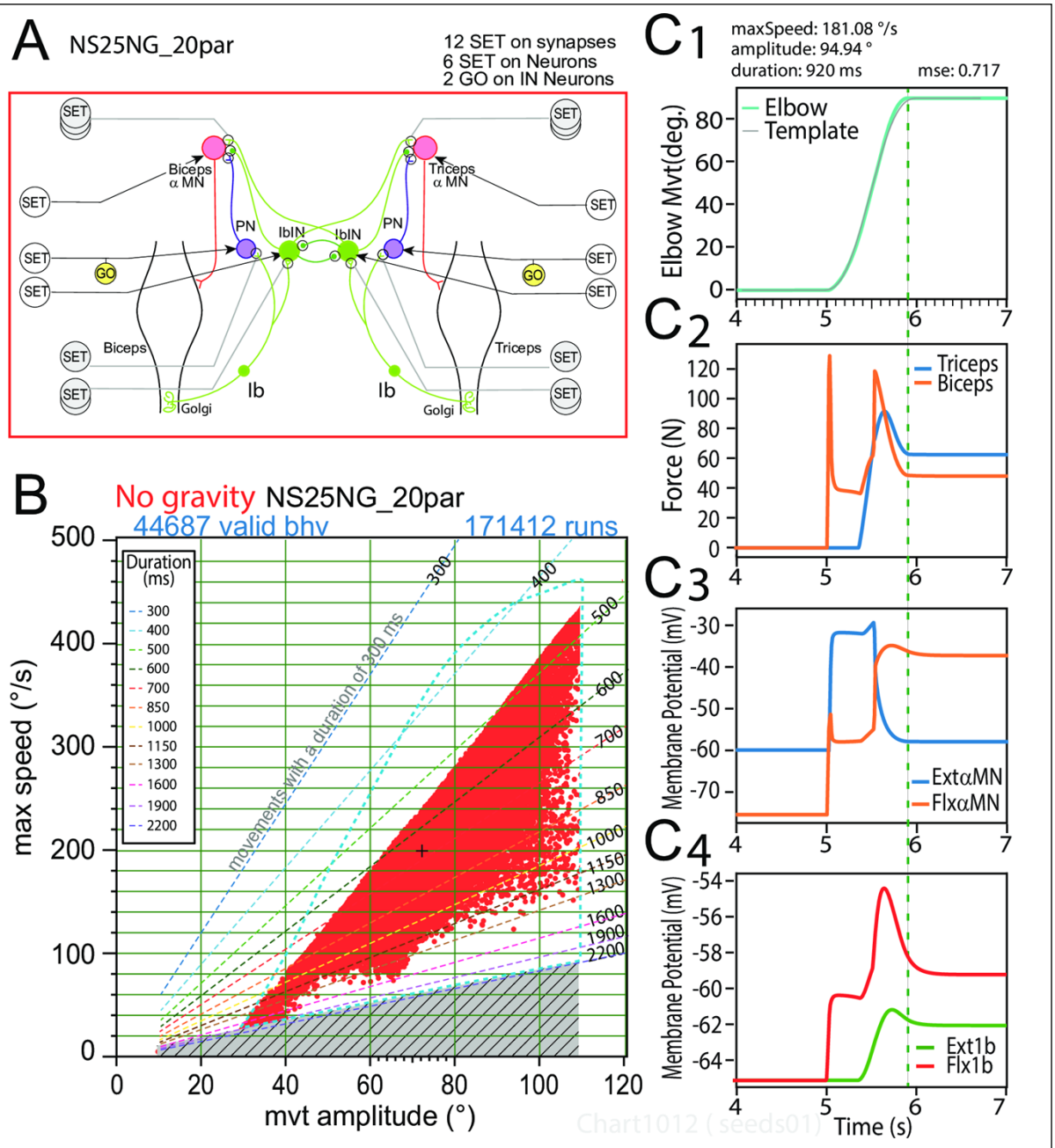

Figure 7: Movements produced by rGEP with the 20-parameters model. **A**, Sensorimotor spinal network of the 20-parameters model. **B**, Behavior domain uncovered by rGEP on this model. For comparison, the perimeter of the domain of the 50-parameter domain is represented with blue dashed line. **C**, Representative example of one valid movement in the behavior domain.

9. Behavioral domain produced in the absence of Ia feedback without central cross-connections.

We also tried a simpler model with Golgi Tendon Organ feedback, in which no cross relationship was present (Figure 8A). This model that was equivalent to the 14-paramaters model for spindles (see Figure 5A), did not produce any valid behavior.

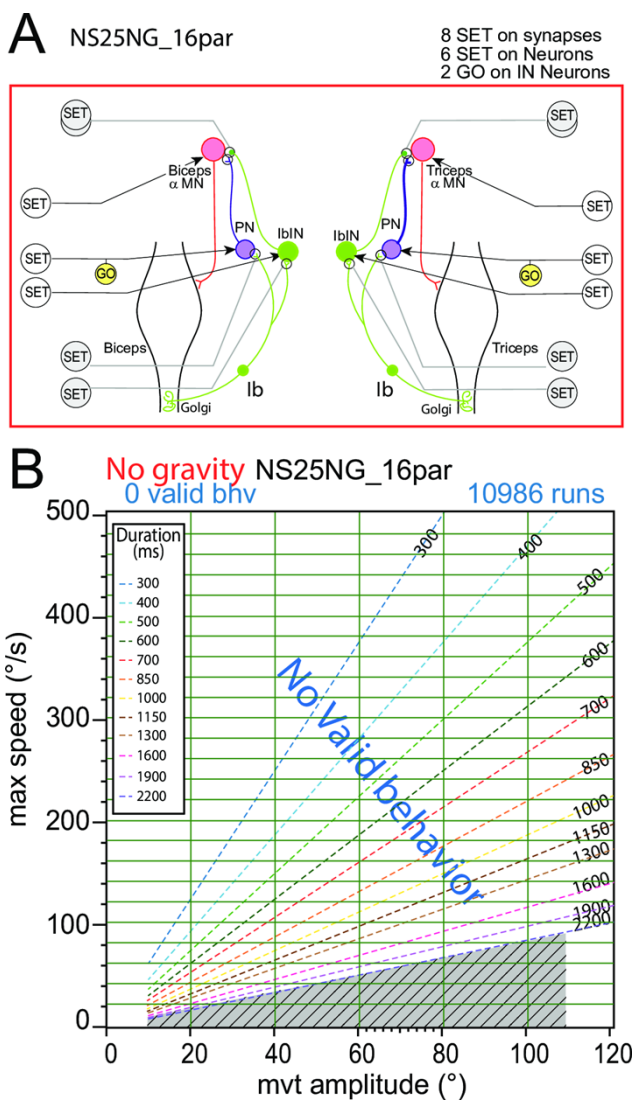

Figure 8: Absence of Valid Movements produced by rGEP with the 16-parameters model. **A**, Sensorimotor spinal network of the 16-parameters model. **B**, Absence of any valid behavior in the behavior domain uncovered by rGEP on this model

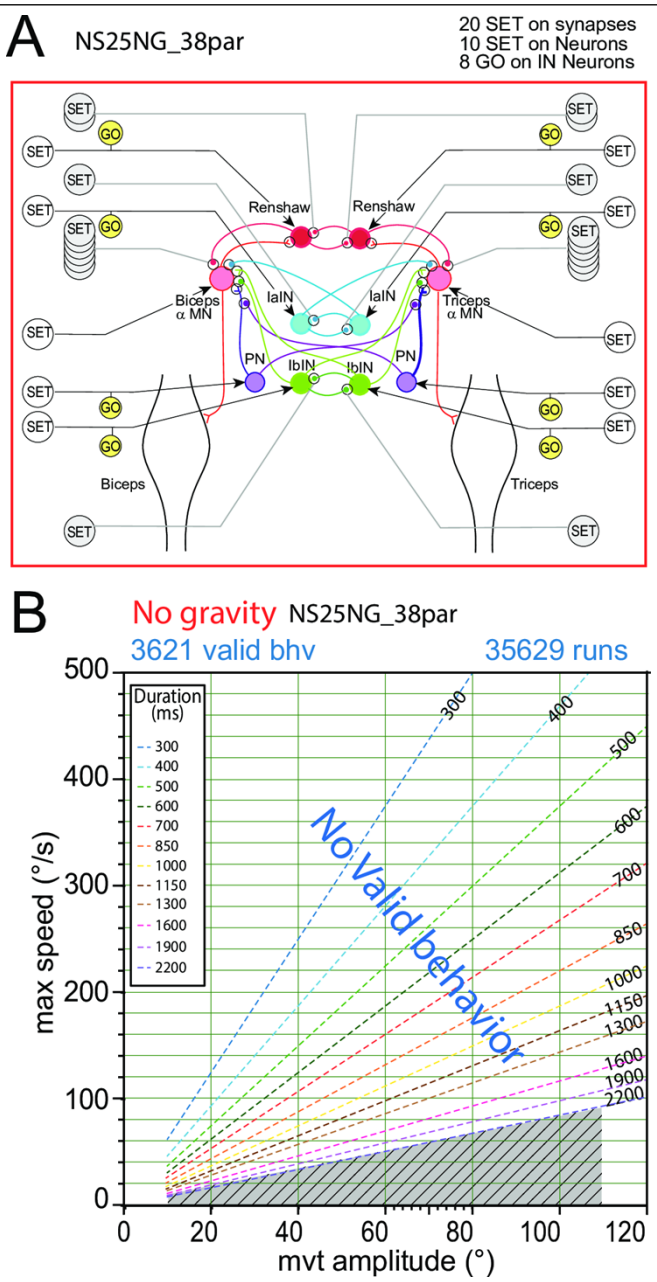

Figure 9: Absence of Valid Movements produced by rGEP with a complete model deprived of proprioceptive feedback. **A**, Sensorimotor spinal network of the 38-parameters model. **B**, Absence of any valid behavior in the behavior domain uncovered by rGEP on this model

413 *10. Behavioral domain produced in the absence of any feedback but with all INs.*

414 Because reciprocal connections seemed important to perform valid behaviors, we
415 tested if complete spinal network deprived of any proprioceptive feedback (Figure 9) could
416 produce valid behaviors. However, no valid behaviors were found with this model (Figure
417 9B).

418 ## B. Analysis of triphasic patterns in the various models.

419 By design, valid behaviors found by rGEP followed the minimum jerk rule. However,
420 as we will see, this rule does not imply conformity with a triphasic command. Triphasic
421 command is defined from the EMG recordings of two antagonistic muscles that were
422 involved in a rapid movement around a joint (**Wachholder 1928; Angel 1974; Wadman et al.**
423 **1979**). Typically, the agonist muscle produced two bursts of activity: one (AG1) at the onset
424 of movement and one (AG2) at end of the movement. The amplitude of the initial agonist
425 burst (AG1) was larger than that of the second (AG2) (**Bullock and Grosberg, 1992**). In
426 between the two agonist bursts, an antagonist burst (ANT) is present (**Sanes and Jennings,**
427 **1984**), the role of which is to slow down the movement speed so that, ideally, the speed is 0
428 when target angle is reached. However, in rapid movements, the activity of the antagonistic
429 muscle is too large and the movement goes back. This effect is counteracted by AG2. This
430 excess of ANT activity and the second burst of the agonist (AG2) produce a small oscillation
431 of the joint angle. Such small oscillations at the movement end were accepted as long as the
432 error (SEM) calculated between the movement and its minimum-jerk profile was less than 1.
433 Movements with too large end oscillation (see Figure 1F, right, profile (1)) were rejected.

434 In order to apply the definition of the triphasic command, we have used the electrical
435 activity of muscles. However, since all models used in this study were based on non-spiking
436 neurons (and hence non-spiking muscle), we used the non-spiking muscle activity to analyze
437 triphasic command occurrences. In order to illustrate EMG profiles, for each model, we give

438 examples of EMGs produced during two small movements (#40°) (one rapid and one slow),
439 during a medium amplitude movement (#60°), and during a large movement (#80°) (see
440 Figure 10B1-4). In addition, given the variety of activity profiles recorded from muscles, we
441 needed to get a measurement of the quality of triphasic pattern. To do this, we defined 3
442 criteria to quantify EMG profiles:

443 • **Criterium 1**: Existence of two agonist (flexor) peaks (AG1, AG2). This was a
444 binary criterium
445 • **Criterium 2**: Existence of antagonist (extensor) peak (ANT) in between AG1
446 and AG2. This was a binary criterium.
447 • **Criterium 3**: Stop of agonist activity between the two peaks. This criterium
448 (name *stopAgonistIndex*) is continuous between 0 (no activity stop) to 1 (total
449 stop of activity between the two peaks).
450 We used the following formula for this calculation:
451 *StopAgonistIndex = 1 - (ANT trough amplitude) / (AG1 peak amplitude)*
452 Each time ANT falls down to -60mV (resting potential), *StopAgonistIndex* takes
453 the value 1. If the relative decrease of the ANT activity between AG1 and AG2
454 (trough) is small (say tending to 0), then *StopAgonistIndex* tends to 0.

455 *1. Triphasic commands with the complete (50-parameters) model*

456 The occurrence of triphasic commands with AG1, ANT, AG2 peaks of activity with the
457 **50-parameters model** (Figure 10A) consisted in the following characteristics: the first AG1
458 flexor peak was generally very prominent (starting at resting potential and reaching a high
459 level of activity (Figure 10B2-4). EMGs were indicated using an arbitrary unit system scale
460 from minimum (0 corresponding to rest) to maximum activity. Its intensity was smaller in
461 slow and small movements (Figure 10B1) compared to fast and large movements (Figure
462 10B2-4). Note however, that the second (AG2) flexor peak was also present but much

smaller (zooming the recording was often needed to make it visible – see Supplementary Figure 1 for more examples with magnification of Flexor activity). The extensor peak of activity (ANT) was regularly present in between the two flexor peaks, although its shape could be complex (see Figure 10B1,3). Note that when the final angle is reached and stable, extensor and flexor activities are maintained at a constant level (that can be different for various movements of the same amplitude, i.e., the equilibrium of torques could be

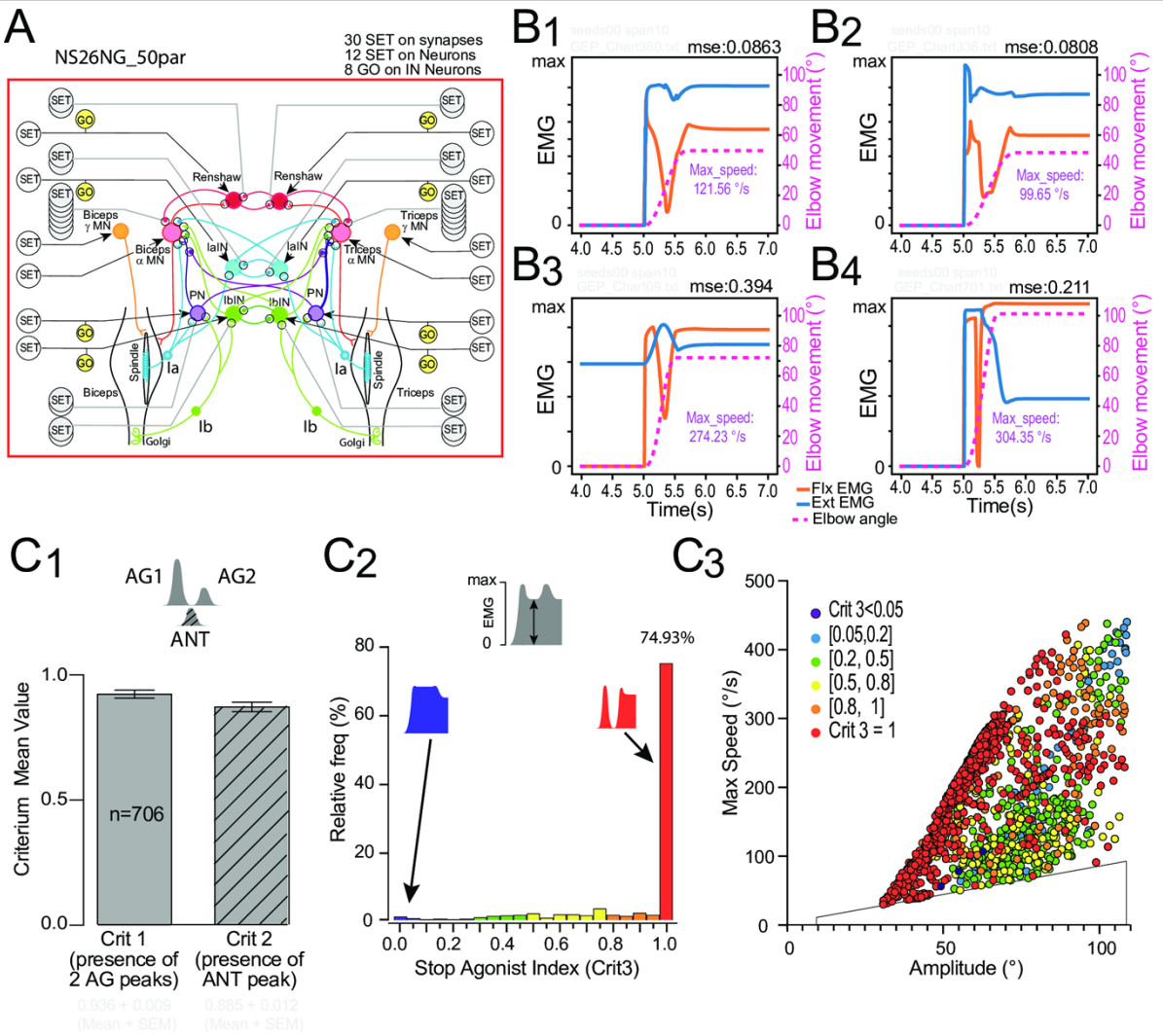

Figure 10: Analysis of triphasic commands occurring in the complete model (50-parameters) with Ia and Ib feedbacks and IN cross-connections. A, Sensorimotor spinal network of the 50-parameters model. **B**, Four representative movements (pink dashed lines) and their corresponding EMG recordings (orange and blue lines for Biceps and Triceps EMGs, respectively). **C**: Estimation of the goodness of the triphasic EMG Command using the three criteria defined in the text. **C1**, Mean value for criteria 1 (Crit 1 - presence of two agonist peaks) and criteria 2 (Crit 2 - presence of antagonist peak), over all valid behaviors of the 50-parameters model. **C2,** Frequency histogram of criterion 3 (AG activity stop between the two AG peaks; crit 3 gives values between 0 (no reduction of AG activity) and 1 (total stop of AG activity) over all valid behaviors, with a majority of total stop (74.93%). **C3**, Distribution of Crit 3 values in the behavior domain (red = total AG block; see color scale).

469 established with various stiffnesses). In between the two flexor peaks (AG1, AG2), the
470 activity of the flexor was totally stopped in most of the valid behaviors obtained with the 50-
471 parameters model (Figure 10B1-4).

472 Based on the criteria define above for triphasic EMG, it appears that the valid
473 behaviors produced by the **compete model** (**50-parameters model**) consisted of a majority
474 of t*riphasic pattern commands* (Figure 10C1). Criterium 1 (presence of two agonist peaks in
475 muscle EMG - AG1 and AG2) and criterium 2 (presence of an antagonist peak ANT in
476 between AG1 and AG2) were satisfied in most of the behaviors (crit1 = 0.936 ± 0.009; crit2 =
477 0.885 ± 0.012; 1 corresponding to 100%, Mean + SEM) (Figure 10C1). The proportion of total
478 stop of the agonist activity (criterium 3) was also very high (74.93% - Figure 10C2), and
479 behaviors displaying this total stop were distributed all over the behavior domain (Figure
480 10C3).

481 *2. Triphasic commands with the with Ia feedback only and cross connections (36-*
482 *parameters model).*

483 Removing the GTO feedback (**36-parameters model**, Figure 11A) did not change
484 fundamentally the occurrence of triphasic commands. It consisted in the presence of the
485 two flexor peaks (AG1, AG2) with a total stop of flexor activity between the two peaks
486 (Figure 11B2-4) and a nice simple extensor peak (ANT) (Figure 11B1-4). Note that the
487 complex shapes of extensor peak observed in Figure 10B1,2,4, were never observed in the
488 36-parameters model (model without GTO feedback).

489 The valid behaviors produced by the compete model deprived of GTO feedback (**36-**
490 **parameters model**) consisted also of a majority of t*riphasic pattern commands* (Figure 11C).
491 Criterium 1 and criterium 3 were satisfied in most of the produced valid behaviors (crit1 =
492 0.981 ± 0.006; crit3 = 0.971 ± 0.008; Mean + SEM) (Figure 11C1). The proportion of total
493 stop of the agonist activity during the antagonist peak (criterium 2) was 53.1% (Figure 11C2),

494 and behaviors displaying this total stop were distributed all over the behavior domain

495 (Figure 11C3).

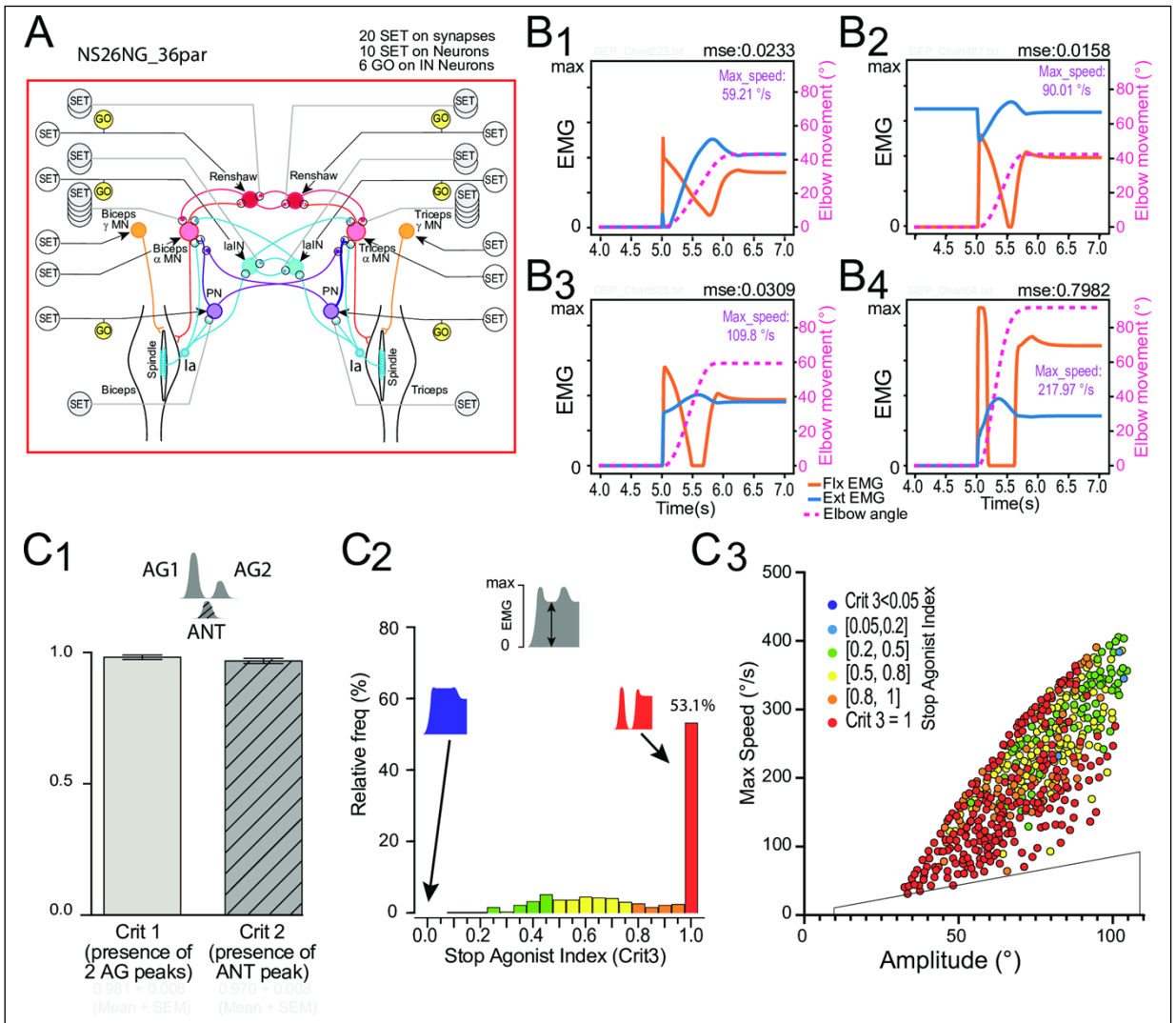

Figure 11: Analysis of triphasic commands occurring in the complex model with Ia feedbacks only and IN cross-connections (36-parameters). A, Sensorimotor spinal network of the 36-parameters model. **B**, Four representative movements and corresponding EMG recordings. **C**: Triphasic criteria (same disposition as in Figure 10).

496 *3. Triphasic commands with only Ia feedback without cross connections (14-*

497 *parameters model).*

498 In the simplest sensorimotor model, without GTO feedback and deprived of

499 Interneurons except PNs (Figure 12A), GEP still produced valid behaviors in a behavior

500 domain almost as large as that of the complete model (compare Figures 6B with Figure 3B).

501 However, the muscle activation patterns (Figure 12B) were more deeply modified compared

502 to that of the complete model. In particular, although the two flexor peaks (AG1, AG2) were

503 present, the activities did not come back to rest (=0 activity) in between (Figure 12B1-4). This

504 was constantly observed whatever the amplitude or speed of the movement (Figure 12B1 4).

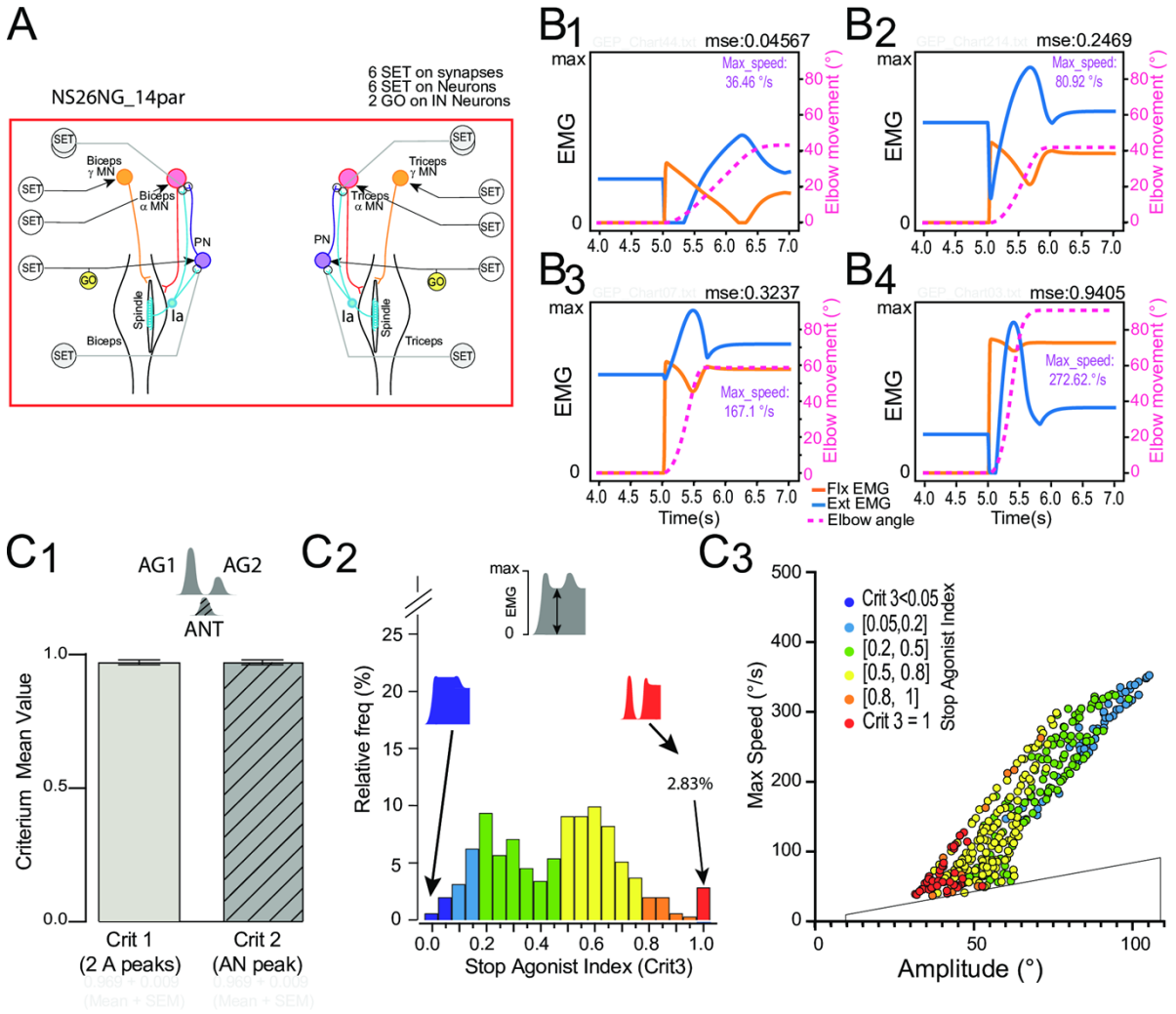

Figure 12: Analysis of triphasic commands occurring in the simple model (14-parameters) with Ia feedbacks only and no IN cross-connections. A, Sensorimotor spinal network of the 50-parameters model. **B**, Four representative movements and corresponding EMG recordings. **C**: Triphasic criteria (same disposition as in Figures 10-11).

505 In this simplest model with Ia feedback only (**14-parameters model**), the presence and

506 disposition of AG1, AG2 and ANT peaks were largely dominant in valid behaviors (Figure

507 12C1). Criterium 1 and criterium 2 were satisfied in most of the produced valid behaviors

508 (crit1 = 0.969 ± 0.009; crit2 = 0.969 ± 0.009; Mean + SEM) (Figure 12C1) (see also

509 Supplementary Figure 2 for more examples with magnification of Flexor activity). The

510 proportion of total stop of the agonist activity during the antagonist peak (criterium 3) was,

511 however, much lower (2.83% - Figure 12C2), with a mean value for Stop_Agonist_Index of

512 0.462 and a median of 0.492. Consequently, it was not possible to estimate the distribution

513 of total agonist stop behaviors in the behavior domain. However, it seems that the
514 distribution of the behaviors with a Stop_Agonist_Index of 1 concerns only small movements
515 (amplitude < 50°); the behaviors with almost total stop (crit3 in range [0.8, 1]) concerns
516 movements < 70°; behaviors with crit3 in the range [0.5, 0.8] (yellow circles) concern
517 movements with an amplitude < 80°. In contrast behaviors with crit3 in the range [0.2, 0.5]
518 (green circles) were distributed all over the behavior domain (Figure 12C3); finally, behaviors
519 with small crit3 values in the range [0.05, 0.2] (blue circles) concern only large movements
520 (amplitude > 60°).

521 *4. Triphasic commands with Ib feedback only and cross connections (34-parameters*
522 *model).*

523 The most complete sensorimotor network deprived from Ia proprioceptive feedback
524 (**34-parameters model**) (Figure 13A) produced a large variety of valid behavior with a
525 behavior domain slightly reduced compared to that of the complete (50-parameters) model
526 (compare Figure 6B with Figure 3B). However, the EMG profile differed from that of the
527 complete 50-parameters model (Figure 13B). In particular, EMG profiles were generally
528 more complex for the flexor activity, with a sharp AG1 peak followed by a plateau of reduced
529 activity (rarely falling down to rest = 0), followed by a second increase of activity with a
530 complex profile (abrupt trough in Figure 13B1; multi stage increase in Figure 13B2). The
531 activity of the Extensor was also deeply modified, with most of the time no clear peak of
532 activity occurring in between the two flexor peaks (Figure 13B1,3), although some behavior
533 presented an increased ANT plateau activity (Figure 13B2. In most cases, the level of activity
534 of the extensor muscle stayed high (close to maximum), or presented a high plateau activity
535 followed by an abrupt decrease before increasing again in a short peak occurring at the
536 same time as AG2 (Figure 13B4).

For this most complete model with Ib feedback only (**34-parameters model**) the mean value of criterium 1 (presence of AG1 and AG2 peaks) was crit1 = **0.639** ± 0.009 (Mean + SEM) (Figure 13C1) against 0.94, 098 and 0.97 for 50-parameters, 36-parameters and 14-parameters models, respectively. Criterium 2 (presence of ANT peak) was greater (Figure 13C1) (crit3=0.854 ± 0.007; Mean + SEM) against 0.885, 0.971 and 0.969 for 50-parameters, 36-parameters and 14-parameters models, respectively. Moreover, for criterium 3, only 2.17% of the valid behaviors displayed a total stop of agonist activity during the ANT peak (Figure 13C2).

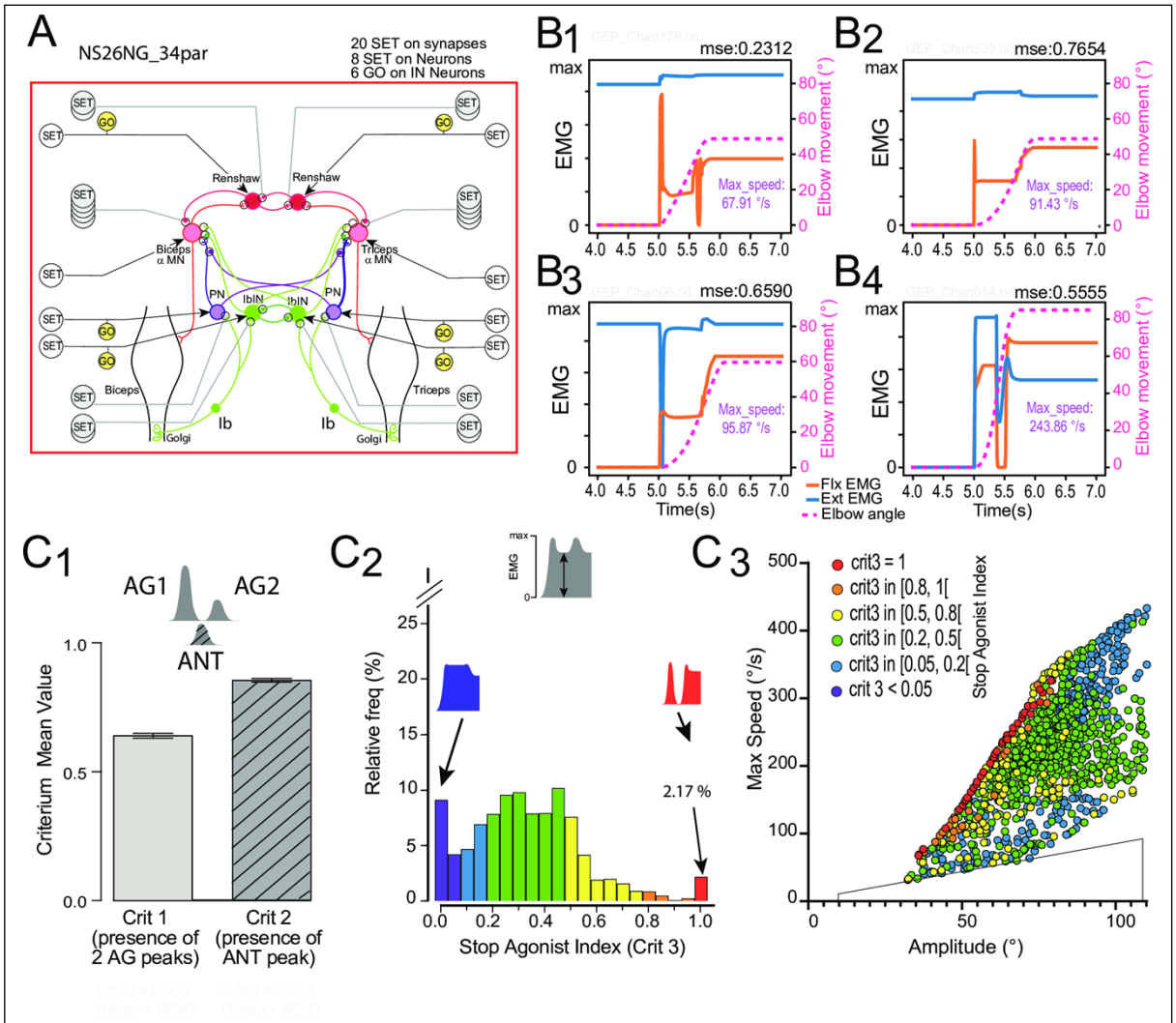

Figure 13: Analysis of triphasic commands occurring in model with Ib afferents only and IN cross-connections. A, Sensorimotor spinal network of the 34-parameters model. **B**, Four representative movements and corresponding EMG recordings. **C:** Triphasic criteria (same disposition as in Figures 10-12).

In addition, the behaviors presenting this total stop of agonist activity were restricted on the highest velocity movements for amplitudes in the range 30-80° (red circles in Figure

547 13C3), while behaviors with a marked trough of agonist activity (crit3 in the range [0.5-0.8])
548 were distributed all over the behavior domain (yellow circles in Figure 13C3), which indicates
549 that less frequent, degraded triphasic pattern can also be produced by the **34-parameters**
550 **model** all over the behavior domain. However, the behaviors with small to absent trough in
551 agonist activity were preponderant all over the behavior domain (blue circles in Figure
552 13C3).

553 *5. Triphasic commands with 1b feedback only and Ib INs cross connections (20-*
554 *parameters model).*

555 In the presence of Ib proprioceptive feedback only, and with Ib INs central cross
556 connections (Figure 14A), the behavior domain was very reduced (Figure 7B) compared to
557 that of the 50-parameters model (Figure 3B). Valid behaviors presented the same
558 characteristics as that of the 34-parameters model (Figure 14B), with a marked brief peak of
559 activity (AG1) (Figure 14B1-4) followed by a reduced plateau activity and a last increase in
560 activity (sometimes with a small AG2 peak– Figure 14B2). The activity of the extensor muscle
561 was generally maintained very high (close to max), sometimes starting at the onset of the
562 SET command (Figure 14B2-3) or starting with the onset of the GO command (Figure 14B1).
563 Nevertheless, there were also behaviors with a peak of activity corresponding to ANT (Figure
564 14B4) .

565 For this simplified **20-parameter model** (with only GTO feedback) (Figure 14A),
566 statistics on triphasic command were close to that of the 14-parameters model. The mean
567 value of criterium 1 (presence of AG1 and AG2 peaks) was crit1 = **0.997** ± 0.002 (Mean +
568 SEM) (Figure 14C1). Criterium 2 (presence of ANT peak) (Figure 14C1) was crit2=**0.855** ±
569 0.011 (Mean + SEM). However, the criterium 3 (stop of agonist discharge during ANT peak)
570 was never encountered (Figure 14C2), the mean value of the Stop Agonist Index being
571 0.316± 0.004 (Mean + SEM). The behavior domain the 20-parameters model (Figure 14C3) is

covered mainly by behaviors with a Stop_Agonist_Index in the range [0.2, 0.5] (Figure 14C3), Behaviors with higher crit3 values are restricted to the smallest movements (see orange and yellow circles).

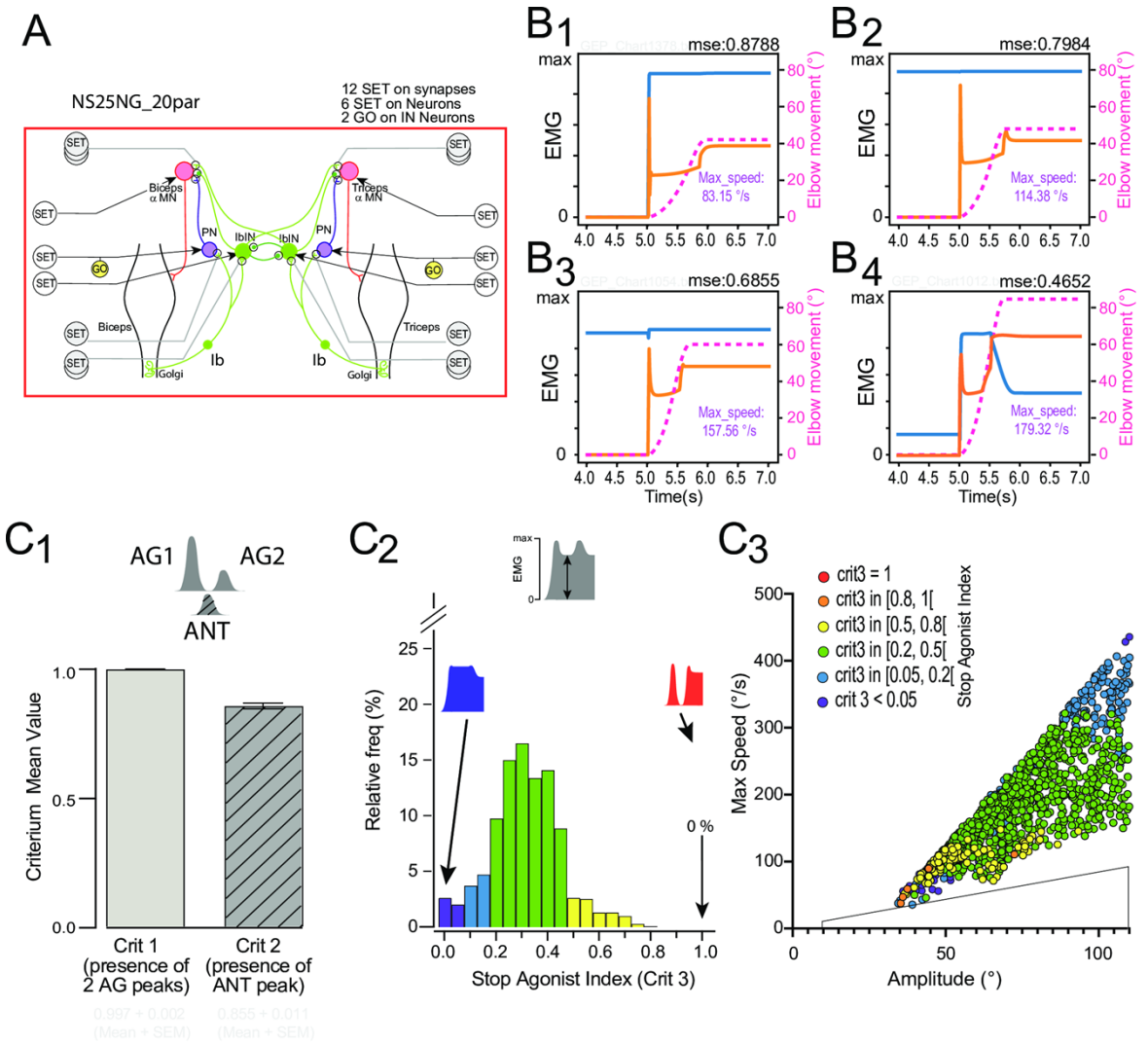

Figure 14: Analysis of triphasic commands occurring in model with Ib afferents only and Ib PN cross connections. A, Sensorimotor spinal network of the 20-parameters model. **B**, Four representative movements and corresponding EMG recordings. **C:** Triphasic criteria (same disposition as in Figures 10-13).

576 # Discussion

577 In the present modelling work, we explored the capacities of spinal sensorimotor
578 networks to produce triphasic EMG pattern when activated by simple descending SET and
579 GO step commands. We observed spontaneously occurring triphasic pattern EMGs produced
580 by spinal sensorimotor circuits (50-parameters model) during the goal exploration process
581 used to establish the behavioral capabilities of the system. Critically, the timing of such
582 triphasic patterns were not predetermined in the descending commands consisting of simple
583 step functions. Particularly, the GO command, initiated the movement (t=5s) but did not give
584 any indication for the observed triphasic EMG patterns. Since the 50-parameters model
585 involved both Ia spindle and GTO afferent feedback, we have used a dissecting out approach
586 to evaluate the role of Ia and Ib afferents and their respective sensorimotor circuits in the
587 elaboration of the triphasic commands.

588 ## A. Role of spindle feedback in triphasic pattern.

589 In the 50-parameters model, most of the valid movements uncovered by the random
590 Goal Exploration Process (rGEP) were triphasic commands (Figure 12A). Removing Ib sensory
591 feedback and Ib sensorimotor circuits did not change much this result (Figure 12B), and
592 indicates that Ia feedback and Ia sensorimotor spinal circuits can handle the elaboration of
593 triphasic commands when descending commands are deprived of such dynamic contains.
594 Moreover, such triphasic commands issued from Ia spindle afferent feedback and Ia
595 sensorimotor spinal circuits are spontaneously produced all over the behavior domain
596 uncovered using the rGEP (Figure 12B3). Note, however, that spinal sensorimotor circuits,
597 and especially reciprocal connections, seem to be important for fast and large valid
598 movements to be produced (compare Figure 5B with Figure 4B). Indeed, the behavior
599 domain is reduced in the absence of these reciprocal connections, but it is still covered by
600 triphasic commands (Figure 12C3) (if we accept only partial stop of agonist discharge

601 between AG1 and AG2 peaks). Yet, it is important to stress that reciprocal connections via
602 spinal interneurons (Renshaw, Ia, Ib, PN) are not sufficient on their own to produce valid
603 movements, i.e., in the absence of proprioceptive feedback (Figure 9). Therefore, this study
604 demonstrates that spindle signals and the associated sensorimotor spinal networks have the
605 capacity to handle the production of triphasic command pattern. It is then highly likely that
606 they participate in the elaboration of this triphasic command in animals and human. But if
607 this conclusion is true, how to explain the finding that triphasic patterns were still produced
608 in transient deafferentation experiments **(Sanes and Jennings 1984)**? In fact, this experiment
609 do not totally invalidate the **participation of sensorimotor circuits** in the shaping of the
610 triphasic command, because the ischemic block affected the afferent activity of the muscles
611 below the elbow, leaving intact both the efferent copy of their motoneurons via Renshaw's
612 interneurons and all proprioceptive feedbacks from all proximal muscles. The widespread
613 extent of these feedback circuits **(Cavallari et al. 1992),** and the strong modulation of
614 proximal muscles to stabilize posture during distal phasic movements, were not fully
615 appreciated until later **(Massion 1992)**.

616 ### B. Role of GTO feedback in triphasic pattern

617 In the absence of Ia feedback, and in the presence of Ib feedback with all Ib
618 sensorimotor circuits, triphasic commands were found all over the corresponding behavior
619 domain (Figure 12D3) which was almost the same as that of the 50-parameters model
620 (compare Figure 6 with Figure 3). However, only 2.17% of movements displayed a total
621 agonist activity block between AG1 and AG2 peaks (see an example of such activity in Figure
622 13B4 and stop agonist index in Figure 13C2). However, the pattern of agonist and antagonist
623 activity was clearly dissimilar from that of the 50-parameters model (i.e., complete model –
624 Figure 10B) and the 36-parameters model (i.e., complete model deprived of Ib feedback –
625 Figure 11B). Indeed, in most valid movements, antagonist activity (Ext EMG) displayed an

626 increased activity at the beginning of the movement (when the GO command starts), and
627 when the ANT peak was present, it occurred at the same time as AG2 (Figure 13B1,B2,B4).
628 This pattern of activity is far from the typical AG1, ANT, AG2 peaks sequence described in
629 **Hallett et al**. (**1975**), in which, even though ANT activity may overlap AG1 or AG2, ANT peak
630 always occurred after AG1 peak and before AG2 peak. For all these reasons, Ib GTO feedback
631 and Ib sensorimotor circuits does not seem to play a central role in the organization of the
632 classical Triphasic command. Note also that the instability resulting from Ib positive feedback
633 onto their MNs is certainly responsible for the complex profiles of EMGs. If we compare the
634 EMG profiles of the 50 parameters model (complete model with Ia and Ib – Figure 10B) with
635 the EMG profiles of the 36-parameters model (complete model deprived from Ib – Figure
636 11B), we note that the instability present in the complete model has disappeared when Ib
637 feedback and sensorimotor circuits have been removed. Nevertheless, Ib GTO feedback
638 seems to play a role in boosting movement initiation, because when Ib feedback is
639 suppressed, Maximal speed is reduced (compare Figure 4B with Figure 3B). This involvement
640 in force enhancement was also described in physiological conditions in cat **(Donelan and**
641 **Pearson 2004)**.

642 ### C. Role of descending commands and spinal networks in triphasic pattern.

643 The fact that Ia spindle feedback and their spinal sensorimotor circuits are capable of
644 handling triphasic commands all over the behavior domain, does not exclude, however, that
645 in physiological conditions, descending command also participate in the elaboration of
646 triphasic commands. Recordings from M1 motor cortex indicate that unit and global
647 activities can be correlated either with static and dynamic forces and torques around single
648 joints **(Cabel et al. 2001)**, or with muscle synergies **(Holdefer and Miller 2002)**. Therefore, it
649 is likely that such precise descending command may interact with spinal sensorimotor
650 networks. In the present report, we used simple step commands to control spinal

651 sensorimotor circuits. Some authors have argued that because EMGs are organized in
652 triphasic pattern with silent periods, this indicated that descending commands did not
653 operate in a smooth and continuous manner **(Leib et al. 2020)**. Indeed, the simple model
654 (bang-bang optimal control model) proposed by these authors is more structured in time
655 than the simple step functions we used here. In the bang-bang control, the control signal
656 abruptly switches between a maximum and a minimum value at certain sparse points in
657 time. The control function is made of three constant segments (with two transitions). The
658 bang-bang model explains both abrupt changes in muscles activity (triphasic command) and
659 the smooth reaching trajectory. Interestingly, rGEP was capable of uncovering a set of valid
660 behaviors (minimum jerk movements) relying incidentally on triphasic commands (with
661 abrupt changes in activity), although this triphasic command was not explicitly searched for
662 nor included in the process with simple step commands. Therefore, it is possible that spinal
663 network properties (and the associated biomechanical effector system) possess the
664 capacities of handling such complex dynamic commands just by giving the correct level of
665 stimulation of target spinal neurons and precise synaptic gain settings. In a more general
666 perspective, these spinal sensorimotor circuits could be considered as the physiological
667 support of movement primitives proposed by **Degallier and Ijspeert (2010)** that can be
668 handled by simple step commands from the brain. In this case, the motor primitives not only
669 encompass movement' start dynamics but also movement' stop dynamics with a unique
670 step command.

671 ### D. Triphasic pattern and minimum jerk.

672 Simulation studies have suggested that minimum-jerk models **(Flash and Hogan**
673 **1985)** and minimum torque-change models **(Uno et al. 1989)** were likely not capable to
674 predict muscle actions **(Osu et al. 2004)** and thus triphasic pattern. Here, we used a different
675 approach that involved a musculoskeletal model associated to spinal sensorimotor

676 networks, and a search method (rGEP) to revisit the capability of spinal sensorimotor circuits
677 to produce triphasic pattern of muscle activation.

678 Indeed, rGEP uncovered a great diversity of parameters associated with a given valid
679 movement. Among these parameters, some will result in triphasic commands. This solution
680 was found all over the behavior domain of the model. But other parameter sets do not fit
681 the definition of triphasic command. For example, although the silence of the agonist
682 between the two agonist peaks (AG1 and AG2) was found in most of the 50-parameters
683 model valid movements (Figure 10B), there were also rare solutions with virtually no
684 reduction in agonist activity (criterion 3<0.05; see violet symbol in Figure 10C3) all over the
685 behavior domain of this complete model. Yet, it seems that triphasic pattern is the natural
686 solution issued from the spinal sensorimotor networks during random Goal Exploration
687 Process (rGEP).

688 The fact that we imposed a minimum jerk profile for movements had consequences
689 on the type of triphasic command retained by rGEP. Indeed, when we consider fast
690 movements that were retained to define the triphasic pattern (**Hallett et al. 1975**), we note
691 the presence of a small oscillation at the end of the movement. The origin of this final
692 oscillation comes from ANT peak that was slightly too strong, resulting in a final oscillation
693 that required the second agonist peak (AG2) to be damped **(Berardelli et al. 1996)**. The
694 minimum jerk profile virtually imposes the absence of such oscillation at the end of the
695 movement, and thereby reduces dramatically the amplitude of AG2 (see blue traces in
696 Figure 10B1-4).

697 ## E. Limits of the study.

698 **No separate Static and Dynamic gamma MNs**. All models of the present study used a
699 mixed type of gamma MN (one for the biceps and one for the triceps). Ideally, we should
700 have used two types of gamma MNs for each muscle: a static gamma MN and a dynamic

701 gamma MN, as was the case in the model of spinal-like regulator **(Raphael et al. 2010)**.
702 However, the activation of the gamma MN of our model increased spindle sensitivity to both
703 position and velocity, and this single type of gamma MN was enough to produce the desired
704 behavior of the model under rGEP. Certainly, the possibility for the descending step
705 commands to act differently on spindle length coding and speed/acceleration coding
706 feedbacks could benefit to the possibilities of control, and likely extend the behavior domain
707 of the model. This point will need future work to estimate the changes brought by the two
708 gamma MN types.

709 **Absence of gravity**. We presented here the results of movements conducted in the
710 absence of gravity. The presence of gravity during elbow flexion exerts an increasing torque
711 that opposes the action of the biceps and could potentially obscure the role of the triceps in
712 slowing down the movement, particularly when the movements are not sufficiently fast. It
713 will be interesting in future investigations to add gravity to see how triphasic pattern evolve,
714 depending on movement trajectory, and how spinal network can handle it. Such studies
715 should show smaller ANT burst when gravity is present and tend to slow down the
716 movement as the forearm becomes more horizontal during flexion movements. Inversely, if
717 movements start from a flexed position (say 110° in our model), and stops at 90°, ANT burst
718 should be dramatically increased.

719 **Simple flexion movement**. In the present study, we used a single joint (elbow) and
720 movement consisted in elbow flexion. This was made because minimum jerk is more
721 adapted to this situation **(Nakano et al. 1999).** It would be interesting to generalize the
722 results of the present study by using more complex models including two joints, and mono-
723 and bi-articular muscles, and considering endpoint reaching movements.

724

Methods

A. Software's used in simulations.

During this work, we have used several models of sensorimotor systems controlling the same musculo-skeletal apparatus. All models were developed with the **AnimatLab software** (https://animatlab.com) (**Cofer et al. 2010)**, a neuromechanical environment based on user-friendly graphic interface that can be downloaded from https://www.animatlab.com. Execution of AnimatLab models can be controlled by **Python scripts**, which were used to command execution of model movements by **descending cues** targeting spinal neurons and synapses (see below). All scripts used in the present work are written in Python3.8 language. For a quick overview of GEP principles, see pseudo script in Supplementary materials. Python scripts for GEP and all simulations included in this study can be downloaded from GitHub, with an installation procedure for all software package involved:

(https://github.com/Cattaert/rGEP/tree/main).

B. Musculoskeletal system

The musculoskeletal model consisted of an upper limb involving an elbow actuated by two antagonistic muscles (biceps and triceps) (Figure 1A). This single musculoskeletal model was used in all simulations, with various spinal sensorimotor circuits and their descending commands (see below). Information about this musculoskeletal model is given in table 1.

745 All movements were produced **in the absence of gravity** in order to avoid natural
746 slowdown of movement speed as the forearm is flexed.

Segments	**Length (mm)**	**density**	**mass**
Humerus	337.0911395	8000 Kg/m3	1.164 Kg
Forearm	283.1808226	8000 Kg/m3	0.802 Kg
Hand	193.21	8000 Kg/m3	0.966 Kg
Joints (coordinates world positions)	**Z_coord (deepness)**	**Y_coord (up-down)**	**X_coord (left-right)**
Elbow	-4.586	-144.65	-5.372
wrist	14.883	-427.07	1.789
Muscle insertions (world positions)			
Biceps origin	0	150.69	26.509
Biceps insertion	-0.578	-188.28	24.146
Triceps origin	0	151.13	-21.51
Triceps insertion	0.934	-103.64	-16.507
Biceps insertion/Forearm elbow axis	52.82947367		
Triceps insertion/forearm elbow axis	42.85182289		

Table 1: musculo-skeletal model data. Coordinates and dimensions are given in mm. The origin of coordinates (0,0,0) is the center of the Humerus, that is in vertical position at rest (see Fig. 1A).

747 ## C. Modelling coding properties of muscle spindle

748 Muscle spindles were added to each muscle. In AnimatLab (see Methods), muscle
749 spindles have the same "attachments" as the muscles. Their tension-length ratio, maximum
750 force capacity, and viscoelasticity are based on the Hill muscle model **(Scovil and Ronsky**
751 **2006)**. To assess the quality of this neuro-musculoskeletal model, imposed movements of
752 flexion and extension were simulated, while muscle spindle activity was recorded (Figure
753 15A). Our first work was to adjust by hand the muscle spindle parameters that controlled
754 their coding of movements so that their response were comparable to electrophysiological

755 data from the literature **(Boyd et al. 1977)** (Figure 15B), in the absence and in the presence

756 of activation of a Gamma MN.

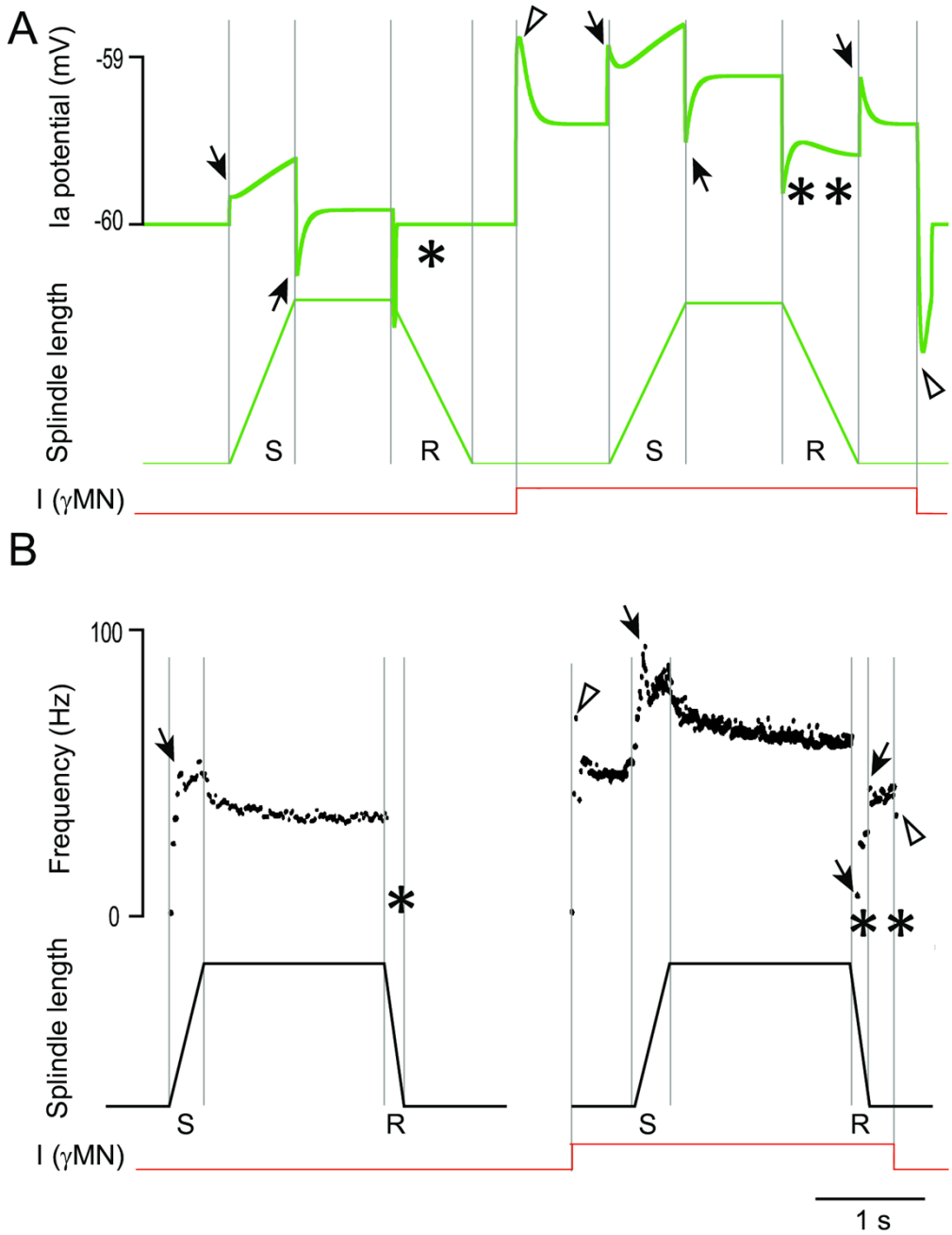

Figure 15. Muscle spindle coding properties

A. Modeled extensor muscle spindle activity during stretch (S) and release (R) ramps, without (left), and with (right) activation of the gamma motoneuron (I γMN). **B.** Electrophysiological recording of the Ia fiber during the same imposed movements as in **A** modified from (**Boyd et al. 1977**)

Note that, in both simulation and physiological recording, the first release of the spindle does not give any response (see *) due to lack of tension of the spindle. However, the activation of the γMN allows the spindle to give an answer during the second release (see **). Note also that in **A**, the "acceleration" component produced by the serial spring velocity (in the Hill model) is responsible for the transient activation at each movement change (arrows), while the "tonic" component produced by the tension of the spindle (in the Hill model) produces an exponential decay shape. Transients are also produced at onset and offset of the γMN stimulation. These features are present in **B** except for transients at the end of stretch movements.

757 ## D. Type of neurons used in the present work

758 Non-spiking (NS) neurons were used to simulate neurons in spinal sensorimotor
759 networks. NS neurons allow a continuous synaptic activation that depends only on
760 presynaptic threshold potential, presynaptic saturation potential, equilibrium potential for
761 post-synaptic effect and synaptic gain (maximal synaptic conductance). The change in
762 postsynaptic conductance increases from 0 (at presynaptic threshold potential) to the
763 maximal synaptic conductance (for presynaptic saturating potential and over). Between
764 these presynaptic threshold and saturation potentials, the postsynaptic conductance
765 increases linearly. Using NS neurons can also be considered as representing population
766 neurons instead of single neurons.

767 ## E. Cost function used to select valid behaviors.

768 For each movement produced, a **cost function** estimated the proximity of
769 movements produced by the simulation to human movement. As normal human movements
770 follow a template based on the minimum jerk model (**Flash and Hogan 1985**), the **cost**
771 **function** calculates the distance (mean square error) between the produced movement and
772 this template (see Figure 1C), with the addition of the penalty for the co-contraction
773 (*Equation 1*). This term was added after a first exploration of the method, which led to
774 systematic co-contraction during the preparation period (result of the SET command). The
775 result was considered valid when the *Loss* value was less than 1.

776

777 $Cost = \sum_{t=2}^{t=10} (T_{desired}(t) - T_{actual}(t))^2 + Penalty\_Prep + Penalty\_Main$ **Equation 1**,

778 with t representing the different sampled times of the simulation (dt=10ms).

779 In order to avoid solutions in which co-contraction occurred during the preparatory
780 phase (or after movement stabilization), co-contraction penalty was added in each of these

781 phases. *Penalty_Prep* was calculated during the preparatory phase (start=2s, end=5s), and
782 *Penalty_Main* during the maintained position phase (start=7s, end=10s). The movement
783 phase was not included because complex interactions may occur due to the dynamics of
784 sensorimotor interactions. The penalty for co-contraction was calculated as indicated in
785 *Equation 2*.

786 $$Penalty\_i = \frac{1}{end - start} * \left(\int_{t=start}^{t=end} (VMN_{flex} - Vthr) * (VMN_{ext} - Vthr) * dt\right) * \ coeff\_i$$ **Equation 2**,

787 in which VMN_{flex} and VMN_{ext} are the membrane potential of the flexor and extensor MNs,
788 respectively, and V_{thr}=-60mV, is a threshold voltage under which penalty = 0.

789 The coefficient (*coeff_i*) was set to 100 during the preparatory phase to make sure
790 coactivation would be rejected in this phase, and *coeff_i* was set to 0 during the maintained
791 position after movement to allow coactivation in this last phase.

792 F. Optimization methods used to get first behaviors (seeds).

793 1. *Variable step coordinate descent (VSCD)*

794 The original method developed by Gerald Loeb's group **(Raphael et al. 2010)** was a
795 classical coordinate descent method, in which all parameters are successively improved
796 individually. The value of each parameter is modified by a given amount (delta) to get a
797 value slightly above and another slightly below the previous setting. A cost value (see cost
798 function above) is calculated for three simulation runs (value above, value below and
799 previous value). The parameter value that elicited the lowest cost value is saved for the next
800 simulation. Then, the process is repeated for the next variable. This method is iterated until
801 the *Loss* value is stable and reaches a minimal value. However, in order to accelerate the
802 optimization process the method was modified : several iterations were performed on each
803 variable before passing to the next one, using an **adaptable delta** inspired from the resilient

804 propagation (Rprop) algorithm **(Igel and Husken 2003).** When iteration improves the loss
805 function, delta value was multiplied by 2.5, and when no improvement was obtained, the
806 delta value was divided by 2 and applied to the previous best iteration to re-center the
807 exploration. We used up to 5 iterations for each parameter. At the end of a round
808 (optimization of all parameters), the order of these variables was shuffled to avoid any order
809 effect that could limit the optimization procedure. For all optimizations, the starting delta
810 was equal to 0.01 which means a variability of 1% of the parameter for the first iteration.

811 *2. Covariance Matrix Adaptation evolution strategy (CMAes)*

812 The second type of optimization algorithm (CMAes) is an evolution algorithm developed
813 by Hansen **(Hansen, 2006)**. It works with a gradient descent with the aim to minimize a cost
814 function. This evolution algorithm is based on the principle of biological evolution. This
815 means that for each generation (iteration), new individuals are generated from variation, in
816 a stochastic way, of the current generation. To initiate the next generation, individuals with
817 the best scores (minimal value of the cost function) are selected to become the parents of
818 the next generation. Following this rule, individuals of the successive generations get closer
819 to the best results.

820 In the evolution algorithm, the solutions that represent the new generations are issued
821 from multivariate-normal distribution based on a variance value (*sigma*) and the covariance
822 matrix of the preceding best solutions. This allows the stochastic changes made to the
823 parameters to be oriented in the direction of the solution. Moreover, from one generation
824 to the next, the *sigma* value is adapted: increased when two generations are in the same
825 direction, and decreased if not. This allows accelerating the progress of optimization.

826 In the CMAes optimization procedure, some parameters have to be given before the
827 simulation was launched including the *limits* of exploration and the *sigma* value. If the *limits*
828 of exploration were too large, new individuals could be generated too far from each other

and the optimal solution might not be reached. A small *sigma* will create a new generation not so different from the previous one and a large one will bring more changes. All optimization series were initiated with a small *sigma* (0.005) and *limits* of exploration covering 100% (i.e., between 0 and 1 for all normalized parameter values). *Sigma* and *limits* were given to CMAes at initiation of optimization process.

Author Contributions

Conceptualization: Daniel Cattaert, Aymar de Rugy, Pierre-Yves Oudeyer.

Funding acquisition:

Methodology: Daniel Cattaert, Bryce Chung, Florent Paclet, Pierre-Yves Oudeyer, Aymar de Rugy.

Project administration: Aymar de Rugy.

Investigation: Daniel Cattaert, Matthieu Guemann.

Software: Daniel Cattaert, Bryce Chung, Florent Paclet.

Supervision: Aymar de Rugy.

Validation: Daniel Cattaert, Aymar de Rugy, Pierre-Yves Oudeyer.

Writing – original draft: Daniel Cattaert.

Writing – review & editing: Daniel Cattaert, Matthieu Guemann, Florent Paclet, Bryce Chung, Pierre-Yves Oudeyer, Aymar de Rugy

Acknowledgments

This work was supported by The Centre National de la Recherche Scientifique (CNRS) and the University of Bordeaux.

852 ## References

853 **Baranes A, and Oudeyer PY**. Active learning of inverse models with intrinsically motivated
854 goal xploration in robots. *Robotics and Autonomous Systems* 61: 2013.

855 **Barnett CH, and Harding D**. The activity of antagonist muscles during voluntary movement.
856 *Ann Phys Med* 2: 290-293, 1955.

857 **Berardelli A, Hallett M, Rothwell JC, Agostino R, Manfredi M, Thompson PD, and Marsden**
858 **CD**. Single-joint rapid arm movements in normal subjects and in patients with
859 motor disorders. *Brain* 119 (Pt 2): 661-674, 1996.

860 **Boyd IA, Gladden MH, McWilliam PN, and Ward J**. Control of dynamic and static nuclear bag
861 fibres and nuclear chain fibres by gamma and beta axons in isolated cat muscle
862 spindels. *J Physiol* 265: 133-162, 1977.

863 **Brown SH, and Cooke JD**. Amplitude- and instruction-dependent modulation of movement-
864 related electromyogram activity in humans. *J Physiol* 316: 97-107, 1981.

865 **Cabel DW, Cisek P, and Scott SH**. Neural activity in primary motor cortex related to
866 mechanical loads applied to the shoulder and elbow during a postural task. *J*
867 *Neurophysiol* 86: 2102-2108, 2001.

868 **Cavallari P, Katz R, and Penicaud A**. Pattern of projections of group I afferents from elbow
869 muscles to motoneurones supplying wrist muscles in man. *Exp Brain Res* 91: 311-
870 319, 1992.

871 **Cofer D, Cymbalyuk G, Reid J, Zhu Y, Heitler WJ, and Edwards DH**. AnimatLab: a 3D graphics
872 environment for neuromechanical simulations. *J Neurosci Methods* 187: 280-288,
873 2010.

874 **Colas C, Sigaud O, and Oudeyer P-Y**. GEP-PG: Decoupling Exploration and Exploita- tion in
875 Deep Reinforcement Learning Algorithms. In: *International Conference on*
876 *Machine Learning (ICML)*. Stockholm, Sweden: 2018.

Degallier S, and Ijspeert A. Modeling discrete and rhythmic movements through motor primitives: a review. *Biol Cybern* 103: 319-338, 2010.

Donelan JM, and Pearson KG. Contribution of force feedback to ankle extensor activity in decerebrate walking cats. *JNeurophysiol* 92: 2093-2104, 2004.

Eliasmith C, and Anderson CH. *Neural engineering : Computation, representation, and dynamics in neurobiological systems.* . MIT press., 2003.

Etcheverry M, Moulin-Frier C, and Oudeyer PY. Hierarchically Organized Latent Modules for Exploratory Search in Morphogenetic Systems. *Advances in Neural Information Processing Systems* 2020.

Eysenbach B, Gupta A, Ibarz J, and Levine S. Diversity is all you need: Learning skills without a reward function. In: *7th Internarional Conference on Learning Representations*. New Orleans, LA, USA, : 2019.

Flash T, and Hogan N. The coordination of arm movements: an experimentally confirmed mathematical model. *J Neurosci* 5: 1688-1703, 1985.

Forestier S, Mollard Y, and Oudeyer P-Y. Intrinsically Motivated Goal Exploration Processes with Automatic Curriculum Learning. arXiv preprint 2017.

Ghez C, and Martin JH. The control of rapid limb movement in the cat. III. Agonist - antagonist coupling. *Exp Brain Res* 45: 115-125, 1982.

Grizou J, Points LJ, Sharma A, and Cronin L. A curious formulation robot enables the discovery of a novel protocell behavior. . *Science advances* 6: 2020.

Hallett M, and Marsden CD. Ballistic flexion movements of the human thumb. *J Physiol* 294: 33-50, 1979.

Hallett M, Shahani BT, and Young RR. EMG analysis of stereotyped voluntary movements in man. *J Neurol Neurosurg Psychiatry* 38: 1154-1162, 1975.

Haruno M, and Wolpert DM. Optimal control of redundant muscles in step-tracking wrist movements. *J Neurophysiol* 94: 4244-4255, 2005.

903 **Holdefer RN, and Miller LE**. Primary motor cortical neurons encode functional muscle
904 synergies. *Exp Brain Res* 146: 233-243, 2002.
905 **Igel C, and Husken MH**. Empirical evaluation of the improved rprop learning algorithms.
906 *Neurocomputing* 50: 105-123, 2003.
907 **Lehman J, and Stanley KO**. Abandoning objectives: evolution through the search for novelty
908 alone. *Evol Comput* 19: 189-223, 2011.
909 **Leib R, Russo M, d'Avella A, and Nisky I**. A bang-bang control model predicts the triphasic
910 muscles activity during hand reaching. *J Neurophysiol* 124: 295-304, 2020.
911 **Massion J**. Movement, posture and equilibrium: interaction and coordination. *Prog*
912 *Neurobiol* 38: 35-56, 1992.
913 **Mouret JB, and Doncieux S**. Encouraging behavioral diversity in evolutionary robotics: an
914 empirical study. *Evol Comput* 20: 91-133, 2012.
915 **Nakano E, Imamizu H, Osu R, Uno Y, Gomi H, Yoshioka T, and Kawato M**. Quantitative
916 examinations of internal representations for arm trajectory planning: minimum
917 commanded torque change model. *J Neurophysiol* 81: 2140-2155, 1999.
918 **Osu R, Kamimura N, Iwasaki H, Nakano E, Harris CM, Wada Y, and Kawato M**. Optimal
919 impedance control for task achievement in the presence of signal-dependent
920 noise. *J Neurophysiol* 92: 1199-1215, 2004.
921 **Oudeyer PY, and Kaplan F**. What is Intrinsic Motivation? A Typology of Computational
922 Approaches. *Front Neurorobot* 1: 6, 2007.
923 **Pathak D, Agrawal P, Efros AA, and Darrell T**. Curiosity-driven exploration by self-supervised
924 prediction. In: *IEEE Conference on Computer Vision and Pattern Recognition*
925 *Workshops* Honolulu, HI, USA: IEEE, 2017, p. 16-17.
926 **Péré A, Forestier S, Sigaud O, and Oudeyer PY**. Unsupervised learning of goal spaces for
927 intrinsically motivated goal exploration. In: *ICLR 2018*2018.

928 **Raphael G, Tsianos GA, and Loeb GE**. Spinal-like regulator facilitates control of a two-
929 degree-of-freedom wrist. *J Neurosci* 30: 9431-9444, 2010.
930 **Reinke C, Etcheverry M, and Oudeyer PY**. Intrinsically Motivated Discovery of Diverse
931 Patterns in Self-Organizing Systems. In: *ICLR 2019*2019.
932 **Rothwell JC, Traub MM, Day BL, Obeso JA, Thomas PK, and Marsden CD**. Manual motor
933 performance in a deafferented man. *Brain* 105 (Pt 3): 515-542, 1982.
934 **Sanes JN, and Jennings VA**. Centrally programmed patterns of muscle activity in voluntary
935 motor behavior of humans. *Exp Brain Res* 54: 23-32, 1984.
936 **Scovil CY, and Ronsky JL**. Sensitivity of a Hill-based muscle model to perturbations in model
937 parameters. *J Biomech* 39: 2055-2063, 2006.
938 **Sergio LE, Hamel-Paquet C, and Kalaska JF**. Motor cortex neural correlates of output
939 kinematics and kinetics during isometric-force and arm-reaching tasks. *J*
940 *Neurophysiol* 94: 2353-2378, 2005.
941 **Terzuolo CA, Soechting JF, and Ranish NA**. Studies on the control of some simple motor
942 tasks. V. Changes in motor output following dorsal root section in squirrel
943 monkey. *Brain Res* 70: 521-526, 1974.
944 **Trainin E, Meir R, and Karniel A**. Explaining patterns of neural activity in the primary motor
945 cortex using spinal cord and limb biomechanics models. *J Neurophysiol* 97: 3736-
946 3750, 2007.
947 **Ueyama Y**. Costs of position, velocity, and force requirements in optimal control induce
948 triphasic muscle activation during reaching movement. *Sci Rep* 11: 16815, 2021.
949 **Uno Y, Kawato M, and Suzuki R**. Formation and control of optimal trajectory in human
950 multijoint arm movement. Minimum torque-change model. *Biol Cybern* 61: 89-
951 101, 1989.

952

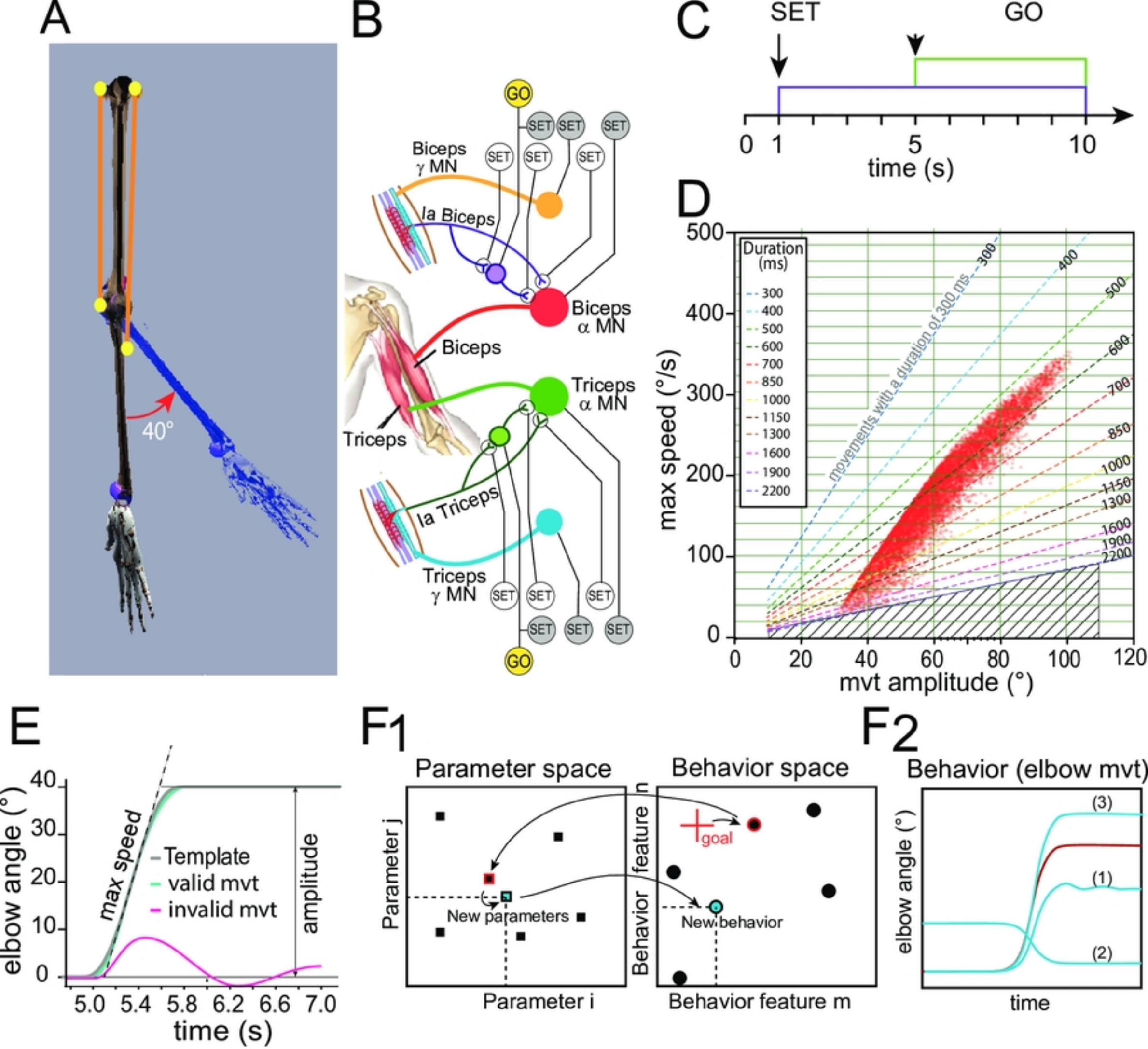
A
40°
B
GO
SET
Biceps
γ MN
Ia Biceps
Biceps
α MN
Biceps
Triceps
α MN
Triceps
Ia Triceps
Triceps
γ MN
C
SET
GO
0
1
5
10
time (s)
D
Duration
(ms)
300
400
500
600
700
850
1000
1150
1300
1600
1900
2200
movements with a duration of 300 ms
max speed (°/s)
mvt amplitude (°)
E
elbow angle (°)
max speed
Template
valid mvt
invalid mvt
amplitude
time (s)
F1
Parameter space
Parameter j
Parameter i
New parameters
Behavior space
Behavior feature n
Behavior feature m
goal
New behavior
F2
Behavior (elbow mvt)
elbow angle (°)
(3)
(1)
(2)
time

Figure01

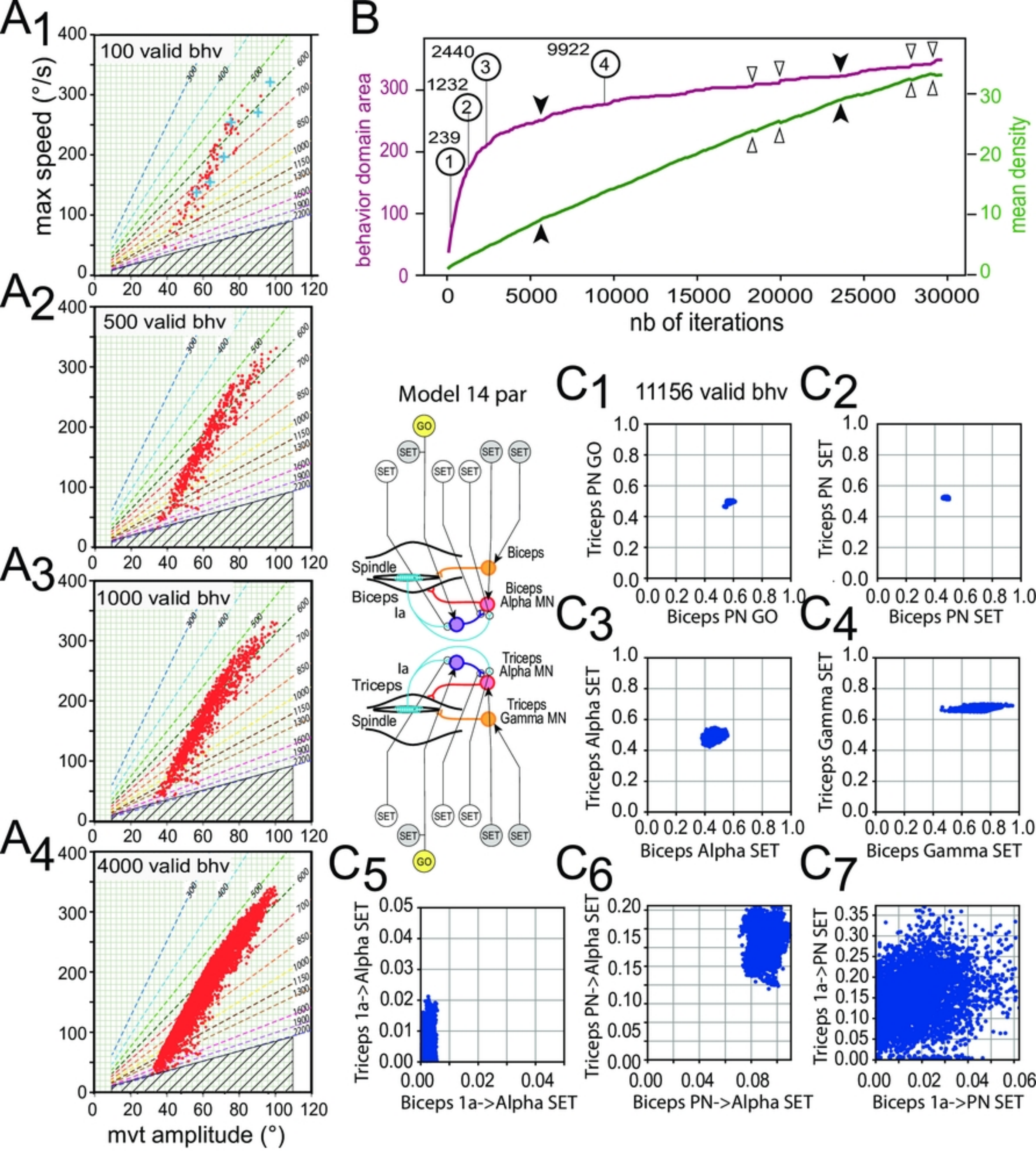
A1
100 valid bhv
max speed (°/s)
A2
500 valid bhv
A3
1000 valid bhv
A4
4000 valid bhv
mvt amplitude (°)
B
behavior domain area
mean density
nb of iterations
2440
9922
1232
239
Model 14 par
GO
SET
Biceps
Spindle
Biceps Ia
Biceps Alpha MN
Triceps Ia
Triceps Alpha MN
Triceps
Triceps Gamma MN
C1
11156 valid bhv
Triceps PN GO
Biceps PN GO
C2
Triceps PN SET
Biceps PN SET
C3
Triceps Alpha SET
Biceps Alpha SET
C4
Triceps Gamma SET
Biceps Gamma SET
C5
Triceps 1a->Alpha SET
Biceps 1a->Alpha SET
C6
Triceps PN->Alpha SET
Biceps PN->Alpha SET
C7
Triceps 1a->PN SET
Biceps 1a->PN SET

Figure02

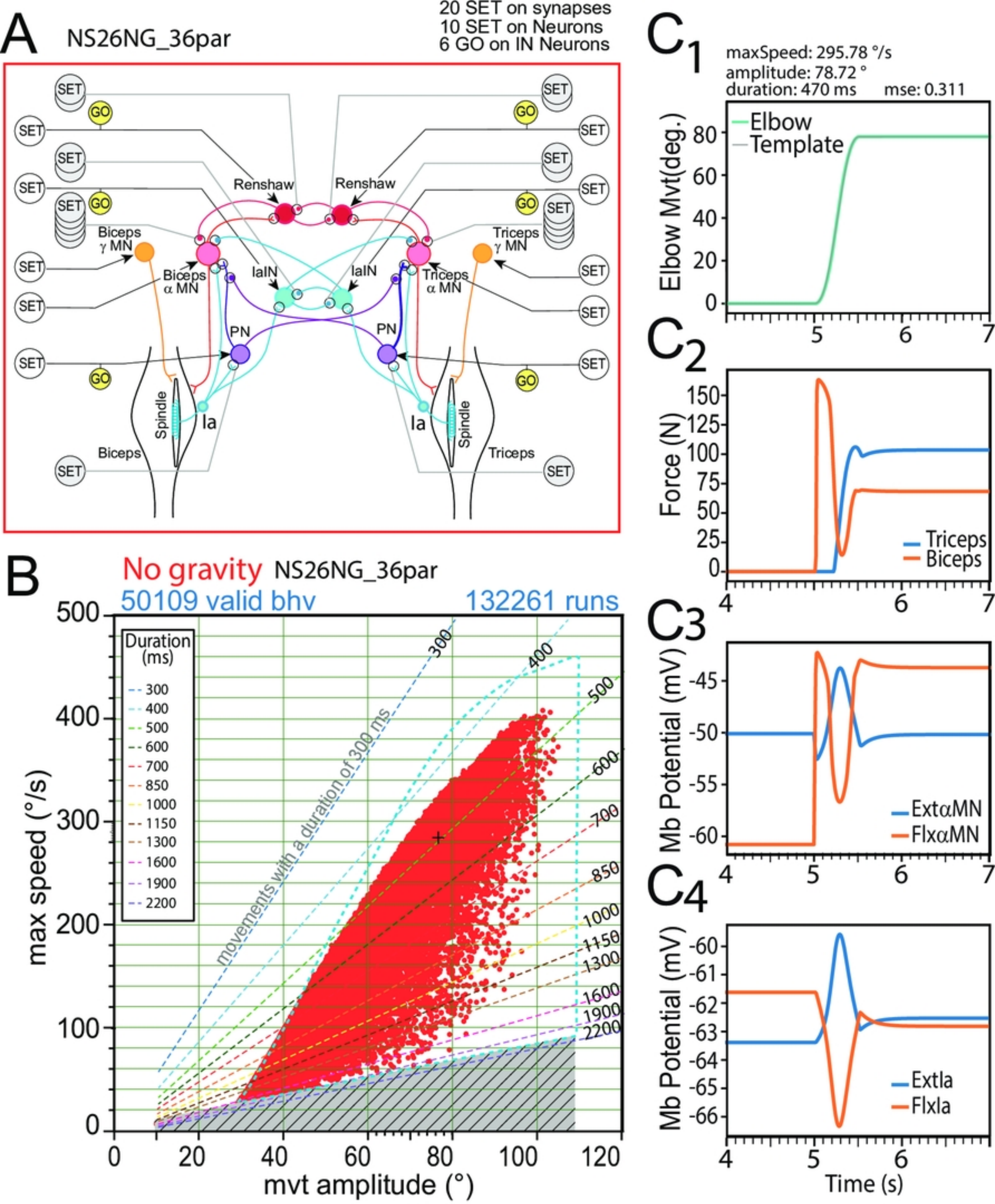
A
NS26NG_36par
20 SET on synapses
10 SET on Neurons
6 GO on IN Neurons
SET
GO
Renshaw
Biceps γ MN
Biceps α MN
Triceps γ MN
Triceps α MN
IaIN
PN
Ia
Spindle
Biceps
Triceps
C1
maxSpeed: 295.78 °/s
amplitude: 78.72 °
duration: 470 ms
mse: 0.311
Elbow
Template
Elbow Mvt(deg.)
C2
Force (N)
Triceps
Biceps
C3
Mb Potential (mV)
ExtαMN
FlxαMN
C4
Mb Potential (mV)
ExtIa
FlxIa
Time (s)
B
No gravity
NS26NG_36par
50109 valid bhv
132261 runs
Duration (ms)
300
400
500
600
700
850
1000
1150
1300
1600
1900
2200
movements with a duration of 300 ms
max speed (°/s)
mvt amplitude (°)

Figure04

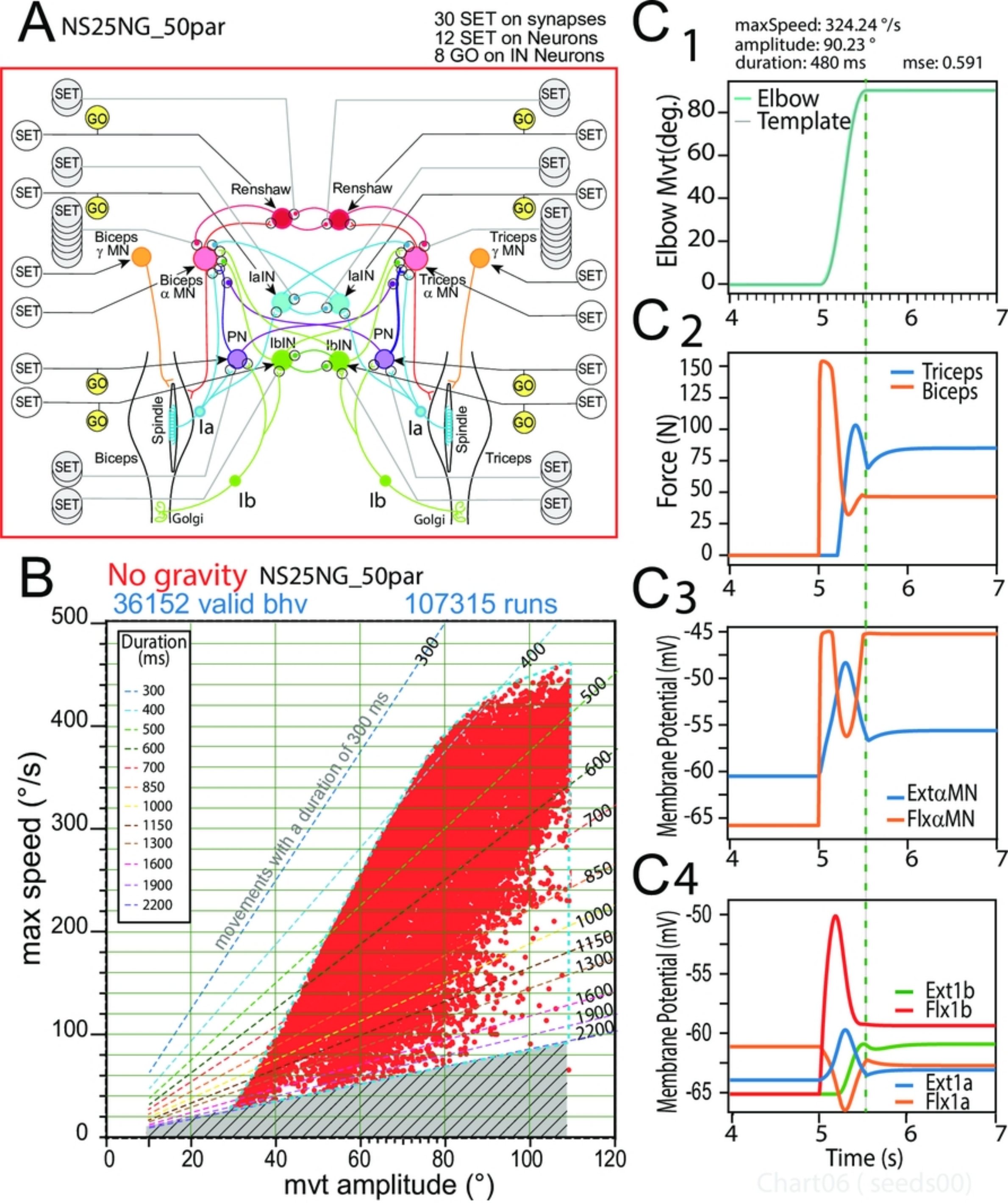
A NS25NG_50par
30 SET on synapses
12 SET on Neurons
8 GO on IN Neurons
SET
GO
Renshaw
Biceps γ MN
Biceps α MN
Triceps γ MN
Triceps α MN
IaIN
PN
IbIN
Spindle
Ia
Ib
Golgi
Biceps
Triceps
B No gravity NS25NG_50par
36152 valid bhv
107315 runs
Duration (ms)
300
400
500
600
700
850
1000
1150
1300
1600
1900
2200
movements with a duration of 300 ms
max speed (°/s)
mvt amplitude (°)
C1
maxSpeed: 324.24 °/s
amplitude: 90.23 °
duration: 480 ms
mse: 0.591
Elbow
Template
Elbow Mvt(deg.)
C2
Triceps
Biceps
Force (N)
C3
ExtαMN
FlxαMN
Membrane Potential (mV)
C4
Ext1b
Flx1b
Ext1a
Flx1a
Time (s)

Figure03

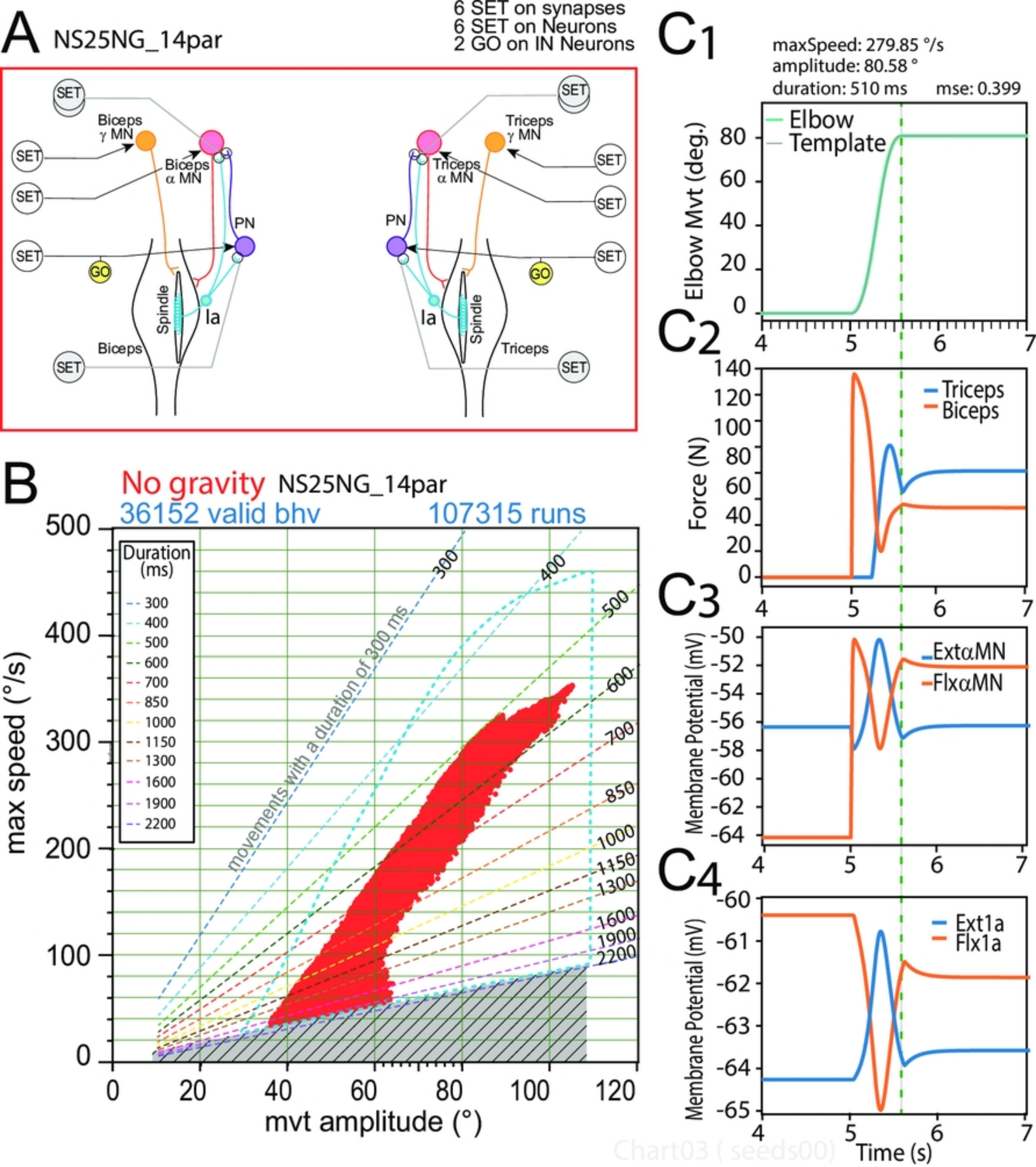
A
NS25NG_14par
6 SET on synapses
6 SET on Neurons
2 GO on IN Neurons
SET
Biceps γ MN
Biceps α MN
PN
GO
Spindle
Ia
Biceps
Triceps γ MN
Triceps α MN
Triceps
B
No gravity
NS25NG_14par
36152 valid bhv
107315 runs
Duration (ms)
300
400
500
600
700
850
1000
1150
1300
1600
1900
2200
movements with a duration of 300 ms
max speed (°/s)
mvt amplitude (°)
C1
maxSpeed: 279.85 °/s
amplitude: 80.58 °
duration: 510 ms
mse: 0.399
Elbow
Template
Elbow Mvt (deg.)
C2
Triceps
Biceps
Force (N)
C3
ExtαMN
FlxαMN
Membrane Potential (mV)
C4
Ext1a
Flx1a
Time (s)

Figure05

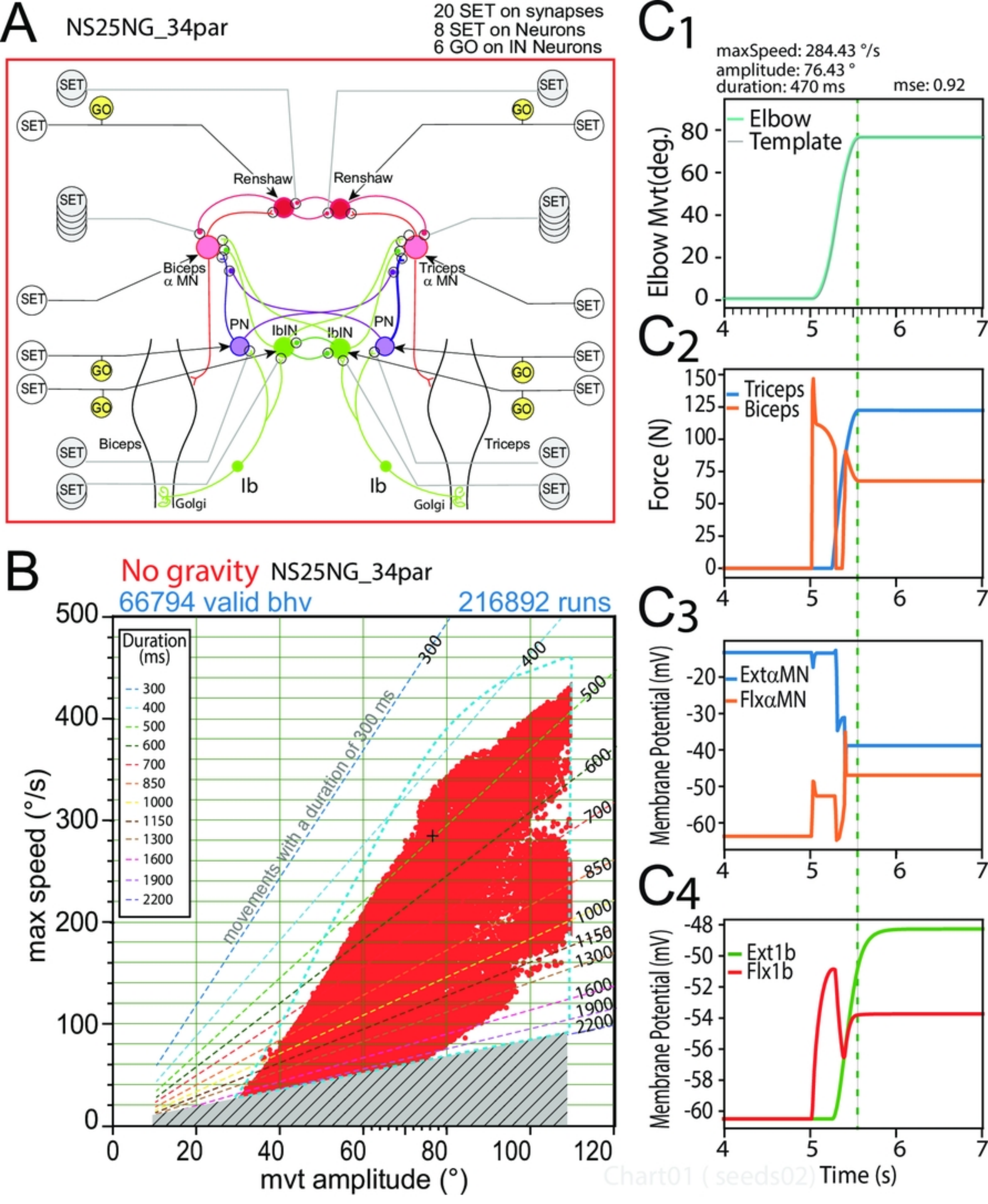
A
NS25NG_34par
20 SET on synapses
8 SET on Neurons
6 GO on IN Neurons
SET
GO
Renshaw
Biceps α MN
Triceps α MN
PN
IbIN
Biceps
Triceps
Ib
Golgi
B
No gravity NS25NG_34par
66794 valid bhv
216892 runs
Duration (ms)
300
400
500
600
700
850
1000
1150
1300
1600
1900
2200
movements with a duration of 300 ms
max speed (°/s)
mvt amplitude (°)
C1
maxSpeed: 284.43 °/s
amplitude: 76.43 °
duration: 470 ms
mse: 0.92
Elbow
Template
Elbow Mvt(deg.)
C2
Triceps
Biceps
Force (N)
C3
ExtαMN
FlxαMN
Membrane Potential (mV)
C4
Ext1b
Flx1b
Membrane Potential (mV)
Time (s)

Figure06

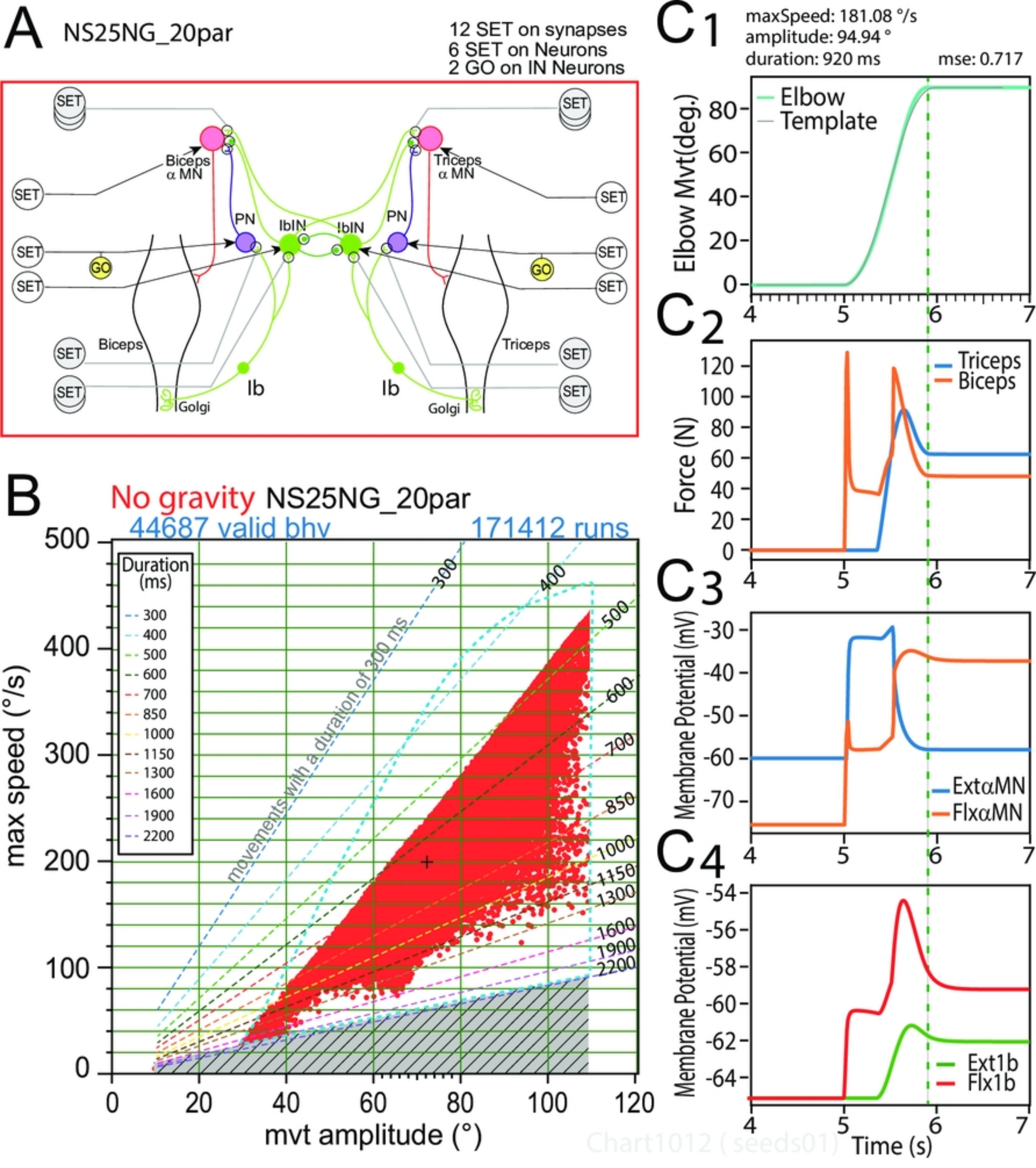
A
NS25NG_20par
12 SET on synapses
6 SET on Neurons
2 GO on IN Neurons
SET
GO
Biceps α MN
Triceps α MN
PN
IbIN
Biceps
Triceps
Ib
Golgi
B
No gravity NS25NG_20par
44687 valid bhv
171412 runs
Duration (ms)
300
400
500
600
700
850
1000
1150
1300
1600
1900
2200
movements with a duration of 300 ms
max speed (°/s)
mvt amplitude (°)
C1
maxSpeed: 181.08 °/s
amplitude: 94.94 °
duration: 920 ms
mse: 0.717
Elbow
Template
Elbow Mvt(deg.)
C2
Triceps
Biceps
Force (N)
C3
Membrane Potential (mV)
ExtαMN
FlxαMN
C4
Ext1b
Flx1b
Time (s)
Chart1012 (seeds01)

Figure07

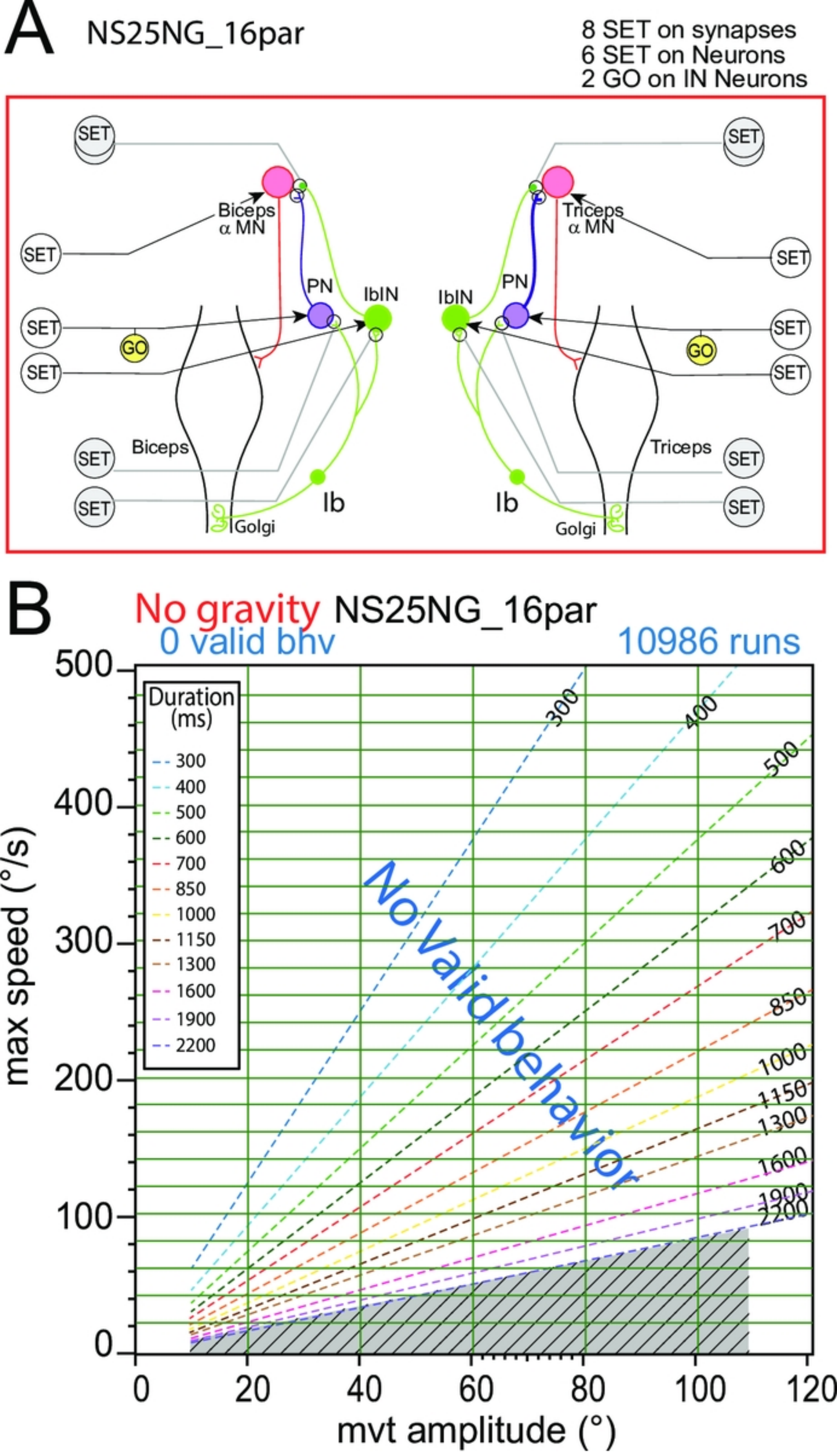
A
NS25NG_16par
8 SET on synapses
6 SET on Neurons
2 GO on IN Neurons
SET
Biceps
α MN
PN
IbIN
GO
Biceps
Ib
Golgi
Triceps
α MN
Triceps
B
No gravity NS25NG_16par
0 valid bhv
10986 runs
Duration (ms)
300
400
500
600
700
850
1000
1150
1300
1600
1900
2200
No Valid behavior
max speed (°/s)
mvt amplitude (°)
0
100
200
300
400
500
0
20
40
60
80
100
120

Figure08

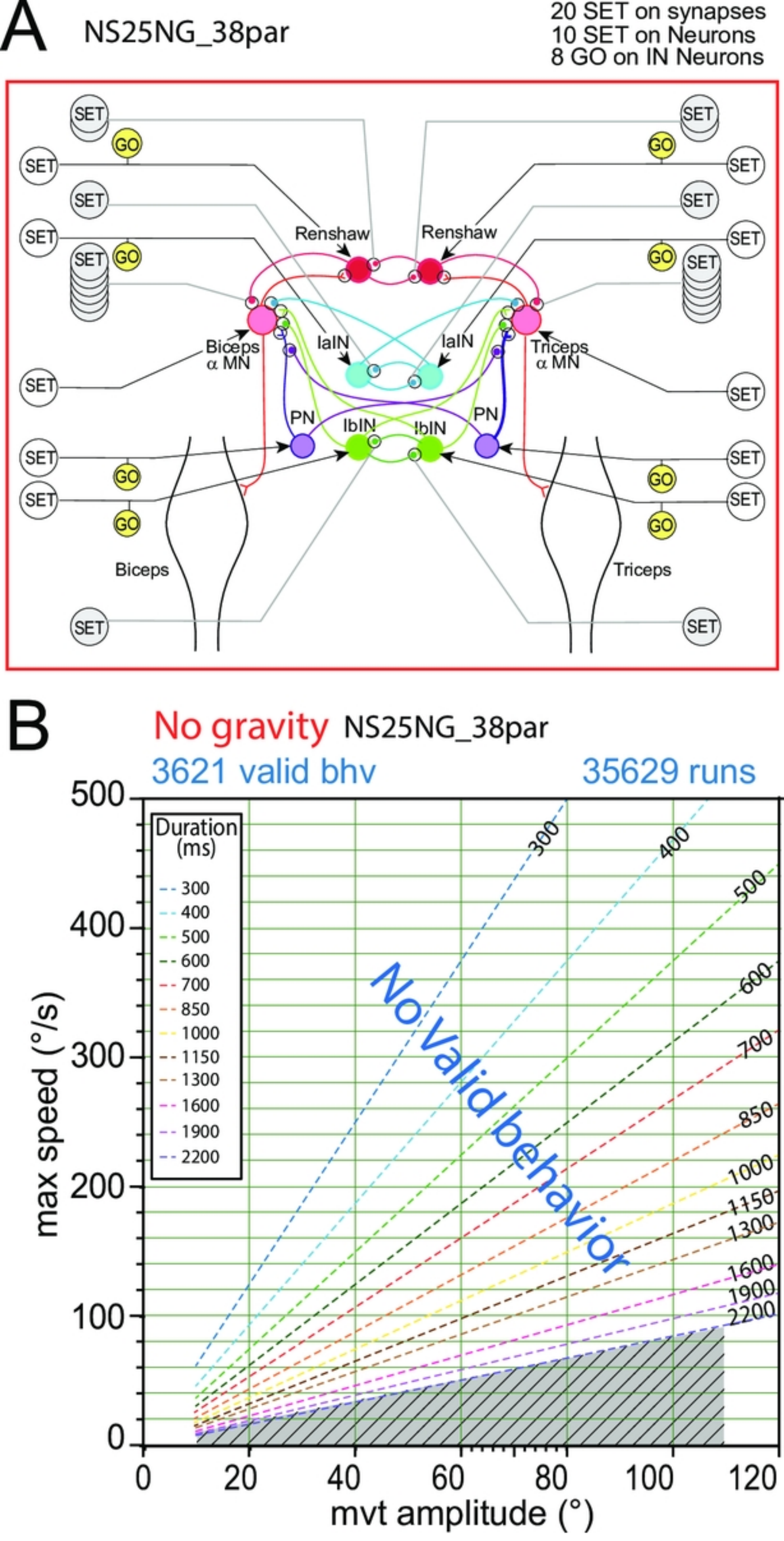
A
NS25NG_38par
20 SET on synapses
10 SET on Neurons
8 GO on IN Neurons
SET
GO
Renshaw
Renshaw
Biceps
α MN
Triceps
α MN
IaIN
IaIN
PN
PN
IbIN
IbIN
Biceps
Triceps
B
No gravity NS25NG_38par
3621 valid bhv
35629 runs
Duration (ms)
300
400
500
600
700
850
1000
1150
1300
1600
1900
2200
No Valid behavior
max speed (°/s)
mvt amplitude (°)
0
100
200
300
400
500
0
20
40
60
80
100
120

Figure09

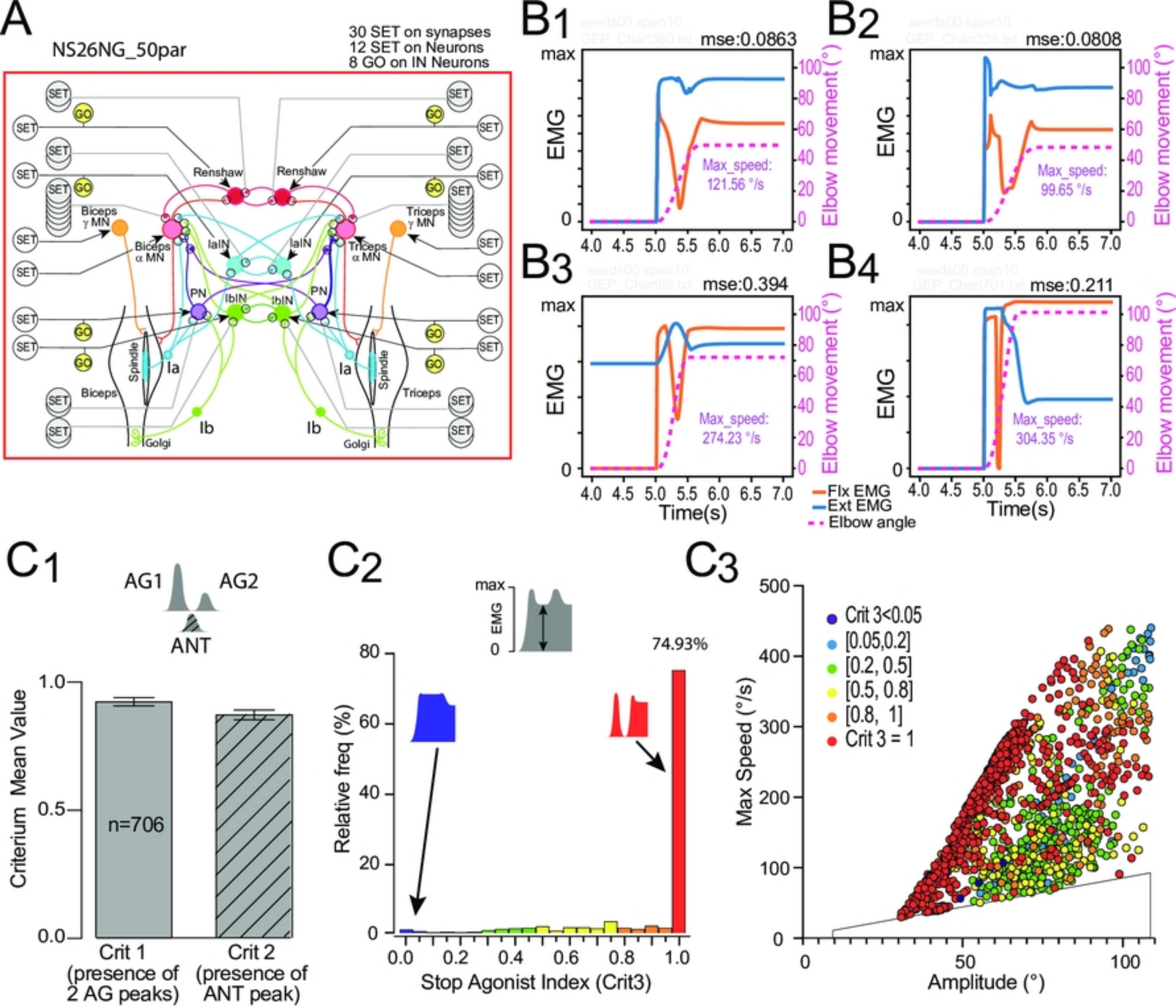
A
NS26NG_50par
30 SET on synapses
12 SET on Neurons
8 GO on IN Neurons
SET
GO
Renshaw
Biceps γ MN
Biceps α MN
Triceps γ MN
Triceps α MN
IaIN
IbIN
PN
Spindle
Ia
Ib
Golgi
Biceps
Triceps
B1
mse:0.0863
Max_speed: 121.56 °/s
B2
mse:0.0808
Max_speed: 99.65 °/s
B3
mse:0.394
Max_speed: 274.23 °/s
B4
mse:0.211
Max_speed: 304.35 °/s
max
EMG
Elbow movement (°)
Time(s)
Flx EMG
Ext EMG
Elbow angle
C1
AG1
AG2
ANT
Criterium Mean Value
n=706
Crit 1 (presence of 2 AG peaks)
Crit 2 (presence of ANT peak)
0.936 + 0.009 (Mean + SEM)
0.885 + 0.012 (Mean + SEM)
C2
Relative freq (%)
74.93%
Stop Agonist Index (Crit3)
C3
Crit 3<0.05
[0.05,0.2]
[0.2, 0.5]
[0.5, 0.8]
[0.8, 1]
Crit 3 = 1
Max Speed (°/s)
Amplitude (°)

Figure10

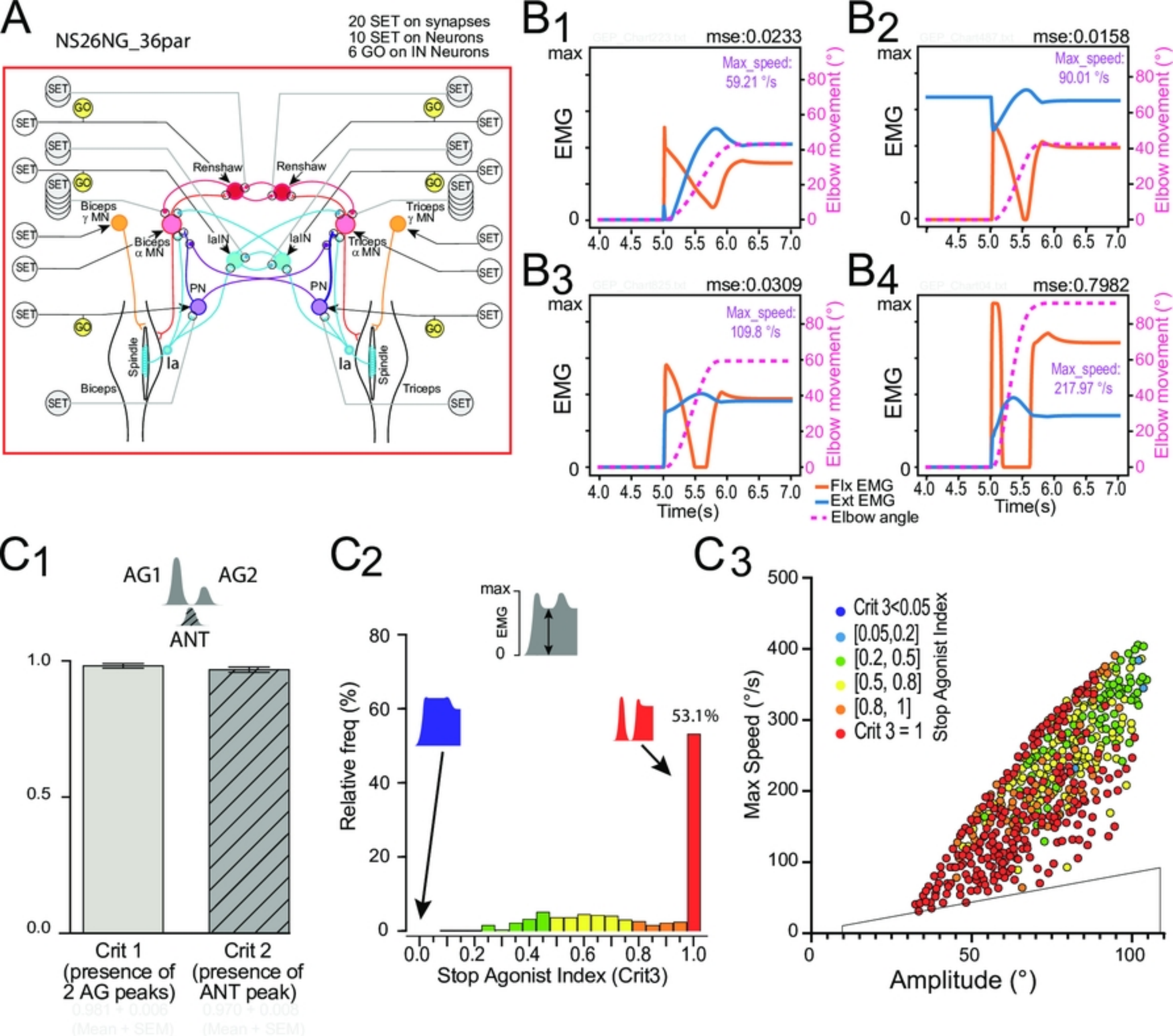
A
NS26NG_36par
20 SET on synapses
10 SET on Neurons
6 GO on IN Neurons
SET
GO
Renshaw
Renshaw
Biceps γ MN
Triceps γ MN
Biceps α MN
Triceps α MN
IaIN
IaIN
PN
PN
Spindle
Ia
Ia
Spindle
Biceps
Triceps
B1
mse:0.0233
Max_speed: 59.21 °/s
B2
mse:0.0158
Max_speed: 90.01 °/s
B3
mse:0.0309
Max_speed: 109.8 °/s
B4
mse:0.7982
Max_speed: 217.97 °/s
max
EMG
Elbow movement (°)
Time(s)
Flx EMG
Ext EMG
Elbow angle
C1
AG1
AG2
ANT
Crit 1 (presence of 2 AG peaks)
Crit 2 (presence of ANT peak)
C2
max
EMG
Relative freq (%)
53.1%
Stop Agonist Index (Crit3)
C3
Crit 3<0.05
[0.05,0.2]
[0.2, 0.5]
[0.5, 0.8]
[0.8, 1]
Crit 3 = 1
Stop Agonist Index
Max Speed (°/s)
Amplitude (°)

Figure11

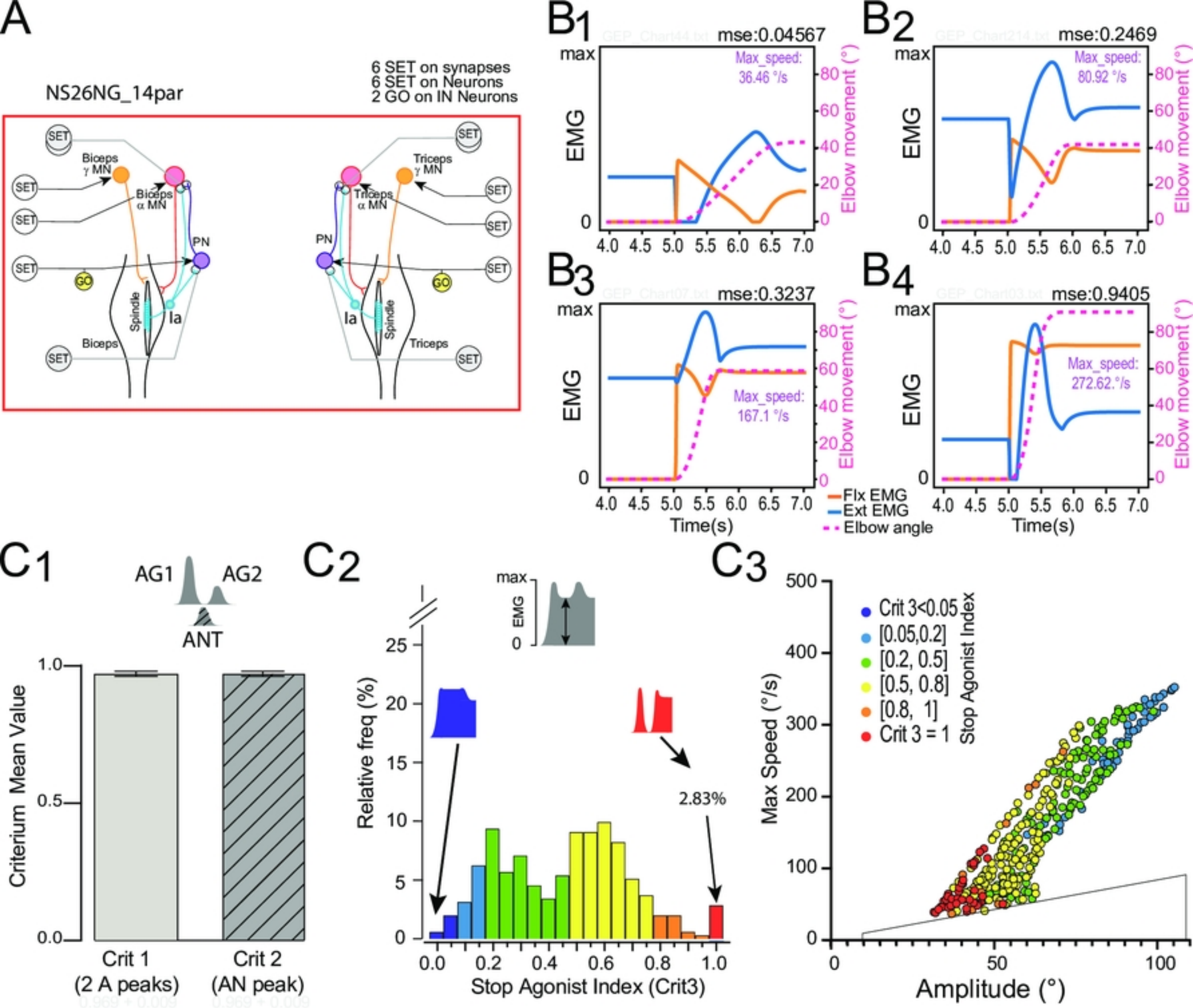
A
NS26NG_14par
6 SET on synapses
6 SET on Neurons
2 GO on IN Neurons
SET
Biceps γ MN
Biceps α MN
PN
GO
Spindle
Ia
Biceps
Triceps γ MN
Triceps α MN
Triceps
B1
mse:0.04567
Max_speed: 36.46 °/s
B2
mse:0.2469
Max_speed: 80.92 °/s
B3
mse:0.3237
Max_speed: 167.1 °/s
B4
mse:0.9405
Max_speed: 272.62 °/s
max
EMG
Elbow movement (°)
Time(s)
Flx EMG
Ext EMG
Elbow angle
C1
AG1
AG2
ANT
Criterium Mean Value
Crit 1 (2 A peaks)
Crit 2 (AN peak)
C2
Relative freq (%)
2.83%
Stop Agonist Index (Crit3)
C3
Crit 3<0.05
[0.05,0.2]
[0.2, 0.5]
[0.5, 0.8]
[0.8, 1]
Crit 3 = 1
Stop Agonist Index
Max Speed (°/s)
Amplitude (°)

Figure12

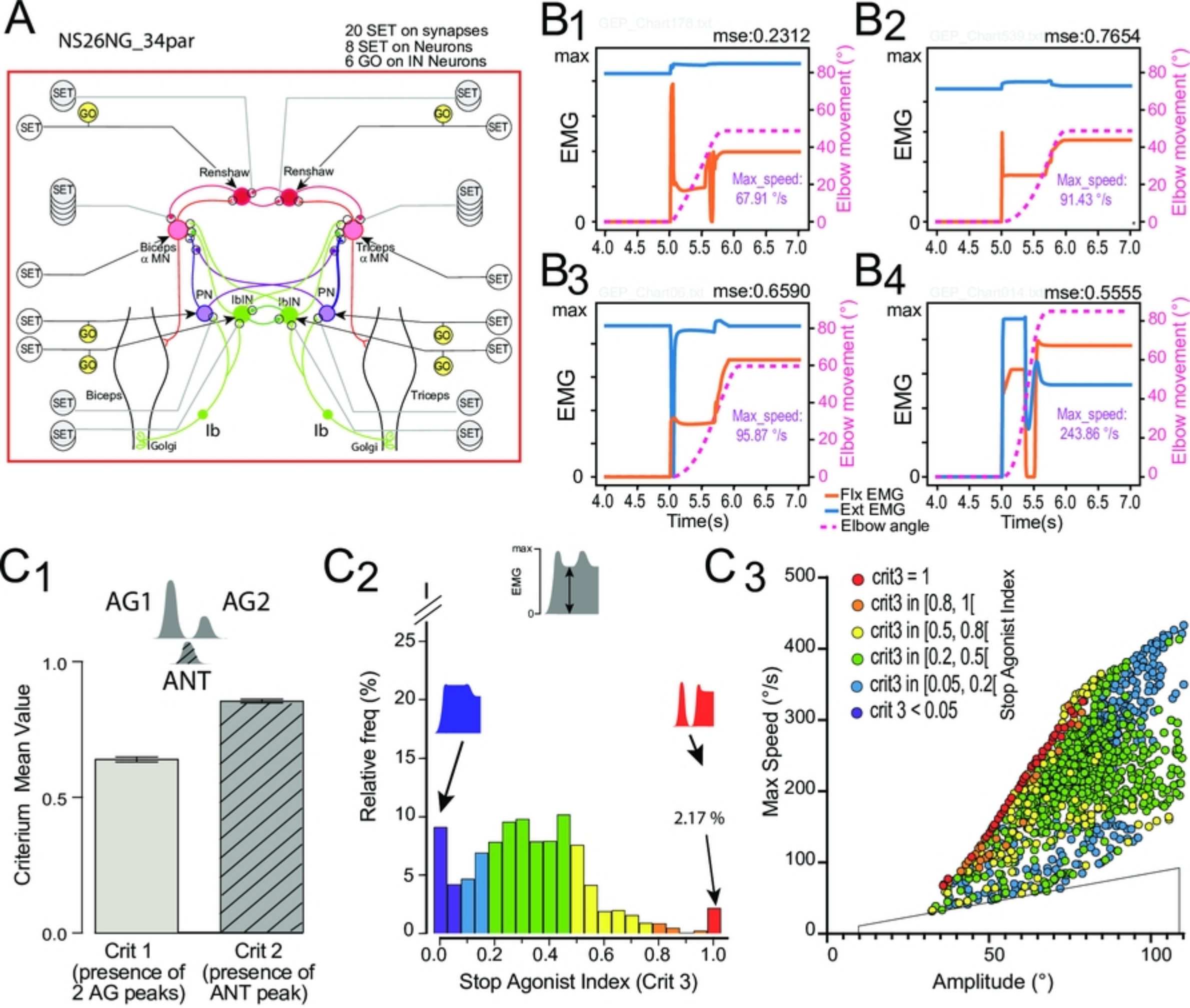
A
NS26NG_34par
20 SET on synapses
8 SET on Neurons
6 GO on IN Neurons
SET
GO
Renshaw
Renshaw
Biceps α MN
Triceps α MN
PN
IbIN
IbIN
PN
Biceps
Triceps
Ib
Ib
Golgi
Golgi
B1
mse:0.2312
Max_speed: 67.91 °/s
B2
mse:0.7654
Max_speed: 91.43 °/s
B3
mse:0.6590
Max_speed: 95.87 °/s
B4
mse:0.5555
Max_speed: 243.86 °/s
max
EMG
Elbow movement (°)
Time(s)
Flx EMG
Ext EMG
Elbow angle
C1
AG1
AG2
ANT
Criterium Mean Value
Crit 1 (presence of 2 AG peaks)
Crit 2 (presence of ANT peak)
C2
Relative freq (%)
2.17 %
Stop Agonist Index (Crit 3)
C3
crit3 = 1
crit3 in [0.8, 1[
crit3 in [0.5, 0.8[
crit3 in [0.2, 0.5[
crit3 in [0.05, 0.2[
crit 3 < 0.05
Stop Agonist Index
Max Speed (°/s)
Amplitude (°)

Figure13

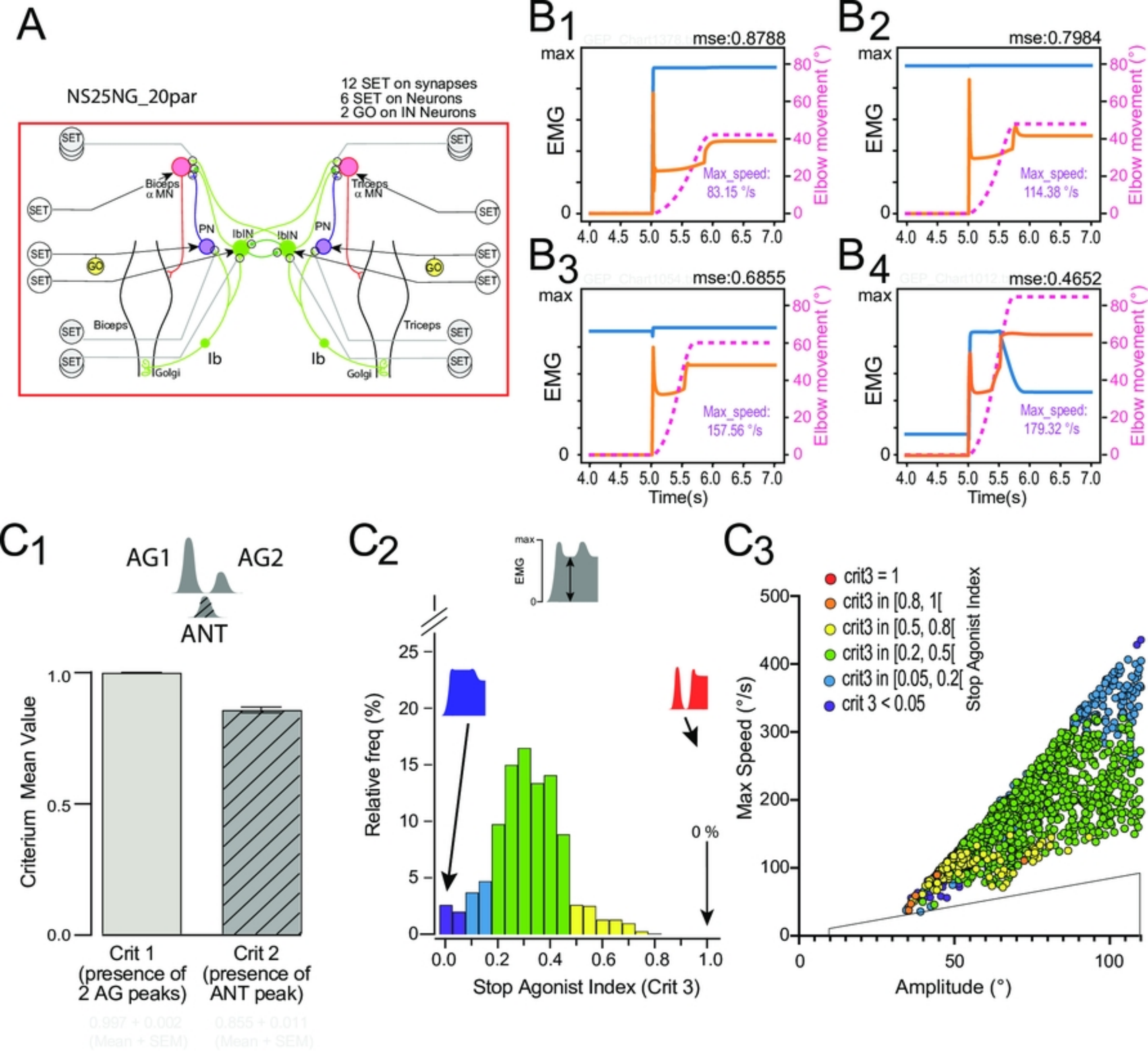
A
NS25NG_20par
12 SET on synapses
6 SET on Neurons
2 GO on IN Neurons
SET
GO
Biceps α MN
Triceps α MN
PN
IbIN
Biceps
Triceps
Ib
Golgi
B1
mse:0.8788
Max_speed: 83.15 °/s
B2
mse:0.7984
Max_speed: 114.38 °/s
B3
mse:0.6855
Max_speed: 157.56 °/s
B4
mse:0.4652
Max_speed: 179.32 °/s
max
EMG
Elbow movement (°)
Time(s)
C1
AG1
AG2
ANT
Criterium Mean Value
Crit 1 (presence of 2 AG peaks)
Crit 2 (presence of ANT peak)
0.997 + 0.002 (Mean + SEM)
0.855 + 0.011 (Mean + SEM)
C2
Relative freq (%)
0 %
Stop Agonist Index (Crit 3)
C3
crit3 = 1
crit3 in [0.8, 1[
crit3 in [0.5, 0.8[
crit3 in [0.2, 0.5[
crit3 in [0.05, 0.2[
crit 3 < 0.05
Stop Agonist Index
Max Speed (°/s)
Amplitude (°)

Figure14

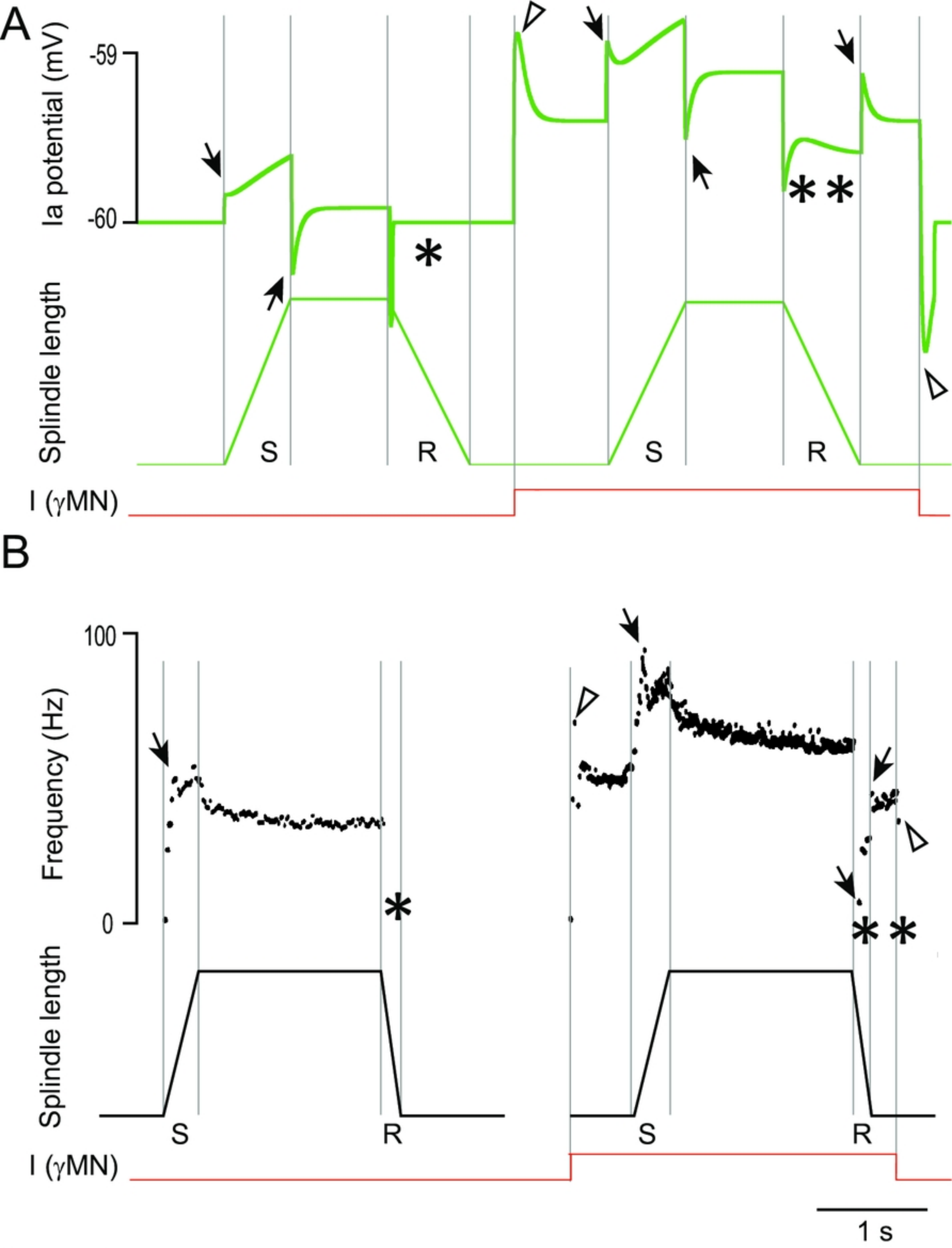
A
Ia potential (mV)
-59
-60
Splindle length
S
R
S
R
I (γMN)
B
100
Frequency (Hz)
0
Splindle length
S
R
S
R
I (γMN)
1 s

Figure15

Model 50 param

Figsup 01

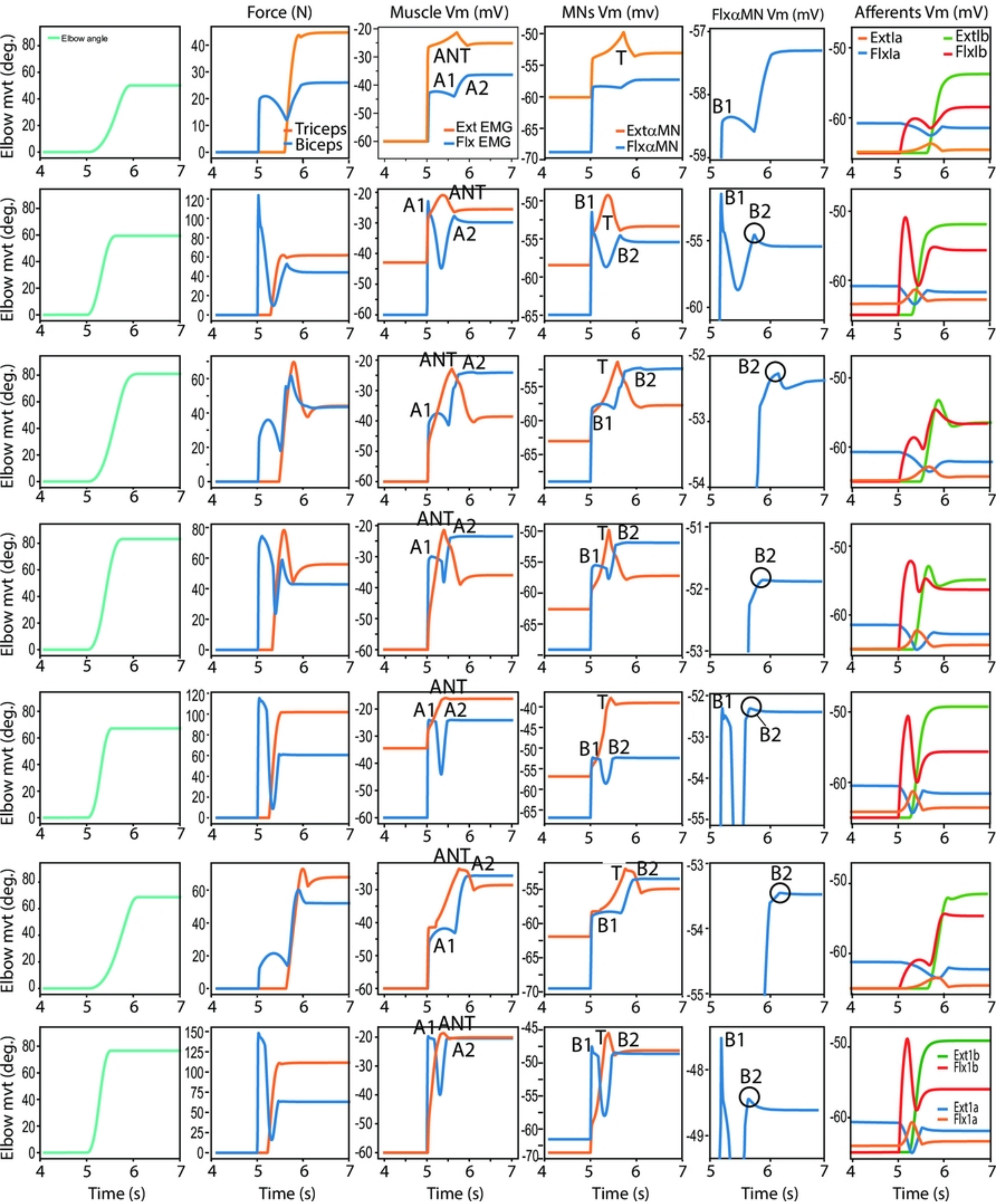

figure Sup01

Model 14 param

Figsup 02

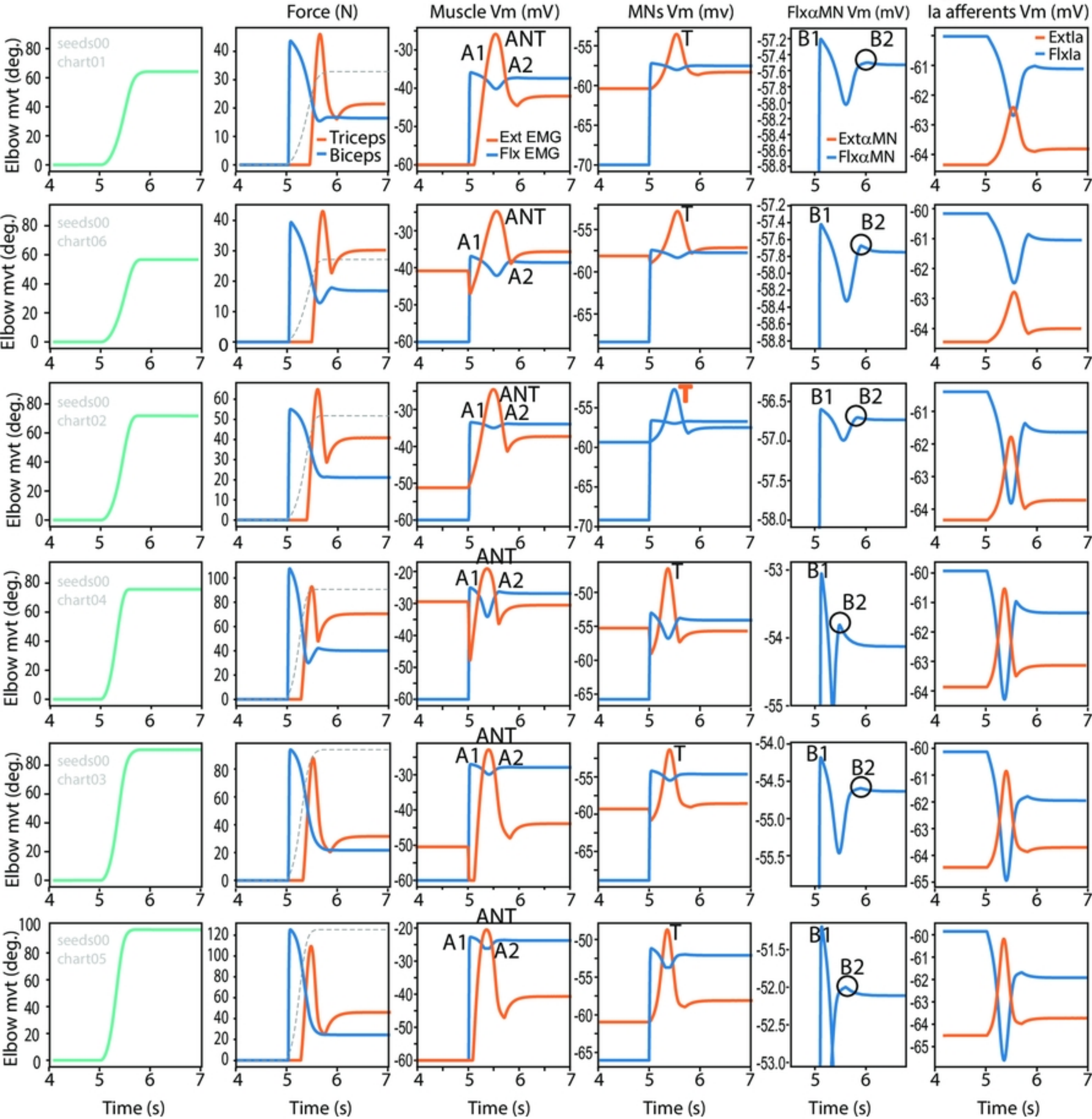

figure Sup02